Supplementary Material to the paper "Fe-Mg partitioning between olivine and high-magnesian melts and the nature of Hawaiian parental liquids" by A.K. Matzen, M.B. Baker, J.R. Beckett, and E.M. Stolper

In this Supplement, we provide four sections intended to amplify and/or expand on specific topics raised in the main text. The first section is an assessment of the data underlying Roeder and Emslie (1970) as given in an unpublished table made available by the senior author. We assess general quality and consider possible sources for the discrepancy in $K_{D,Fe^{+2}\text{-}Mg}$ values between the canonical 0.30 obtained by Roeder and Emslie (1970) and the ~0.34 preferred in this study. Section 2 provides a detailed description of the projection technique used in the main text to reduce compositional dependences of $K_{D,Fe^{+2}\text{-}Mg}$ on melt and olivine composition for literature data. In Section 3, we evaluate the sources of discrepancies between predictions of the Ford *et al*. (1983) and Toplis (2005) models for $K_{D,Fe^{+2}\text{-}Mg}$ and our experimental data. Finally, Section 4 is a listing of all of the references for data incorporated into our database of olivine-liquid pairs from the literature.

1. An Assessment of the Experimental Data of Roeder and Emslie (1970)

1.1. Introduction

Roeder and Emslie (1970) is an enormously influential paper, marking one of the great advances in igneous petrology. By experimentally determining the partitioning of magnesium and iron between olivine and liquid and using an exchange equilibrium involving the two cations, Mg and Fe^{+2}, they showed that the temperature and composition dependences of single-element partitioning between phases largely canceled. Thus, given nothing but the composition of an olivine, it became possible to directly calculate the Mg/Fe^{+2} ratio of the coexisting liquid. By focusing on olivine, Roeder and Emslie (1970) established that even the most common, compositionally simple minerals had a lot to say about their environment of formation.

Although the work of Roeder and Emslie (1970) has provided an intellectual motivation for hundreds of subsequent papers, the vast majority of the experimental data remained unpublished and has, to our knowledge, never been compared quantitatively with later work. At the time the paper was published, the editorial policies at

Contributions to Mineralogy and Petrology were not conducive to printing large data tables and electronic supplements did not exist. Moreover, all of the data used in Roeder and Emslie (1970) were made freely available by the senior author upon request and, indeed, we obtained a copy of the data table (hereafter referred to as REUPDT), nearly forty years after publication.

Our in-depth examination of the data of Roeder and Emslie (1970) was motivated by two of our reviewers who asked us to reconcile the discrepancy between our data and those in the recent literature suggesting that $K_{D,Fe^{+2}\text{-}Mg}$ for Hawaiian basaltic liquids is ~0.34 with the canonical value of 0.30 obtained by Roeder and Emslie (1970). $K_{D,Fe^{+2}\text{-}Mg}$ = 0.30 is still commonly used for generic petrologic calculations and a 0.04 difference in the selected $K_{D,Fe^{+2}\text{-}Mg}$ can have a large effect on the results, so it is important to see if the source of this discrepancy can be inferred. Moreover, because Roeder and Emslie measured FeO and Fe_2O_3 by wet chemistry (albeit on their bulk experimental charges), this discrepancy does not simply reflect a difference in Fe^{+3}/Fe^{+2} algorithm. In section 1.2, we begin our analysis of Roeder and Emslie (1970) by reproducing their calculations. These results establish a quantitative basis for determining the effect of different approaches to analyzing the data on $K_{D,Fe^{+2}\text{-}Mg}$. We also confirm that a facial interpretation of their data using the procedures outlined in Roeder and Emslie (1970) does in fact lead to $K_{D,Fe^{+2}\text{-}Mg} \sim 0.30$. In sections 1.3 through 1.5, we apply our mass balance approach and other tools to evaluate the REUPDT data and discuss the implications of our results for the canonical value of $K_{D,Fe^{+2}\text{-}Mg}$ and the connectivity between results of our study and those of Roeder and Emslie (1970).

1.2. $K_{D,Fe^{+2}\text{-}Mg}$ as determined by Roeder and Emslie (1970)

As a first step towards analyzing the data of Roeder and Emslie (1970), we sought to reproduce their calculation of $K_{D,Fe^{+2}\text{-}Mg}$ as summarized in their Fig. 4. This computation requires four pieces of information, the concentrations of MgO and FeO in the olivine and the concentrations of MgO and FeO in liquid. Roeder and Emslie (1970) used electron microprobe analyses for both oxides in olivine (only forsterite and fayalite contents are given in REUPDT but these are readily converted to oxides). For the liquid, Roeder and Emslie (1970) determined MgO and FeO* (i.e., total Fe as FeO) from

electron microprobe analyses of the glass but there are no direct analyses of FeO and, although wet chemical measurements were made of FeO (and Fe_2O_3), these were done on bulk splits, not on glass separates. Thus, prior to calculating a value for $K_{D,Fe^{+2}\text{-}Mg}$, FeO for the whole sample had to be disaggregated into FeO residing in olivine and FeO in the liquid. Roeder and Emslie (1970) approached this problem through mass balance using MgO in olivine and glass, assuming that only these two phases contributed to bulk MgO. From the relative weights of the two phases, they then partitioned the known bulk FeO between liquid and olivine, also assumed to be present only in these two phases, and computed $K_{D,Fe^{+2}\text{-}Mg}$. Roeder and Emslie (1970) used the results of 27 experiments for this purpose (22 on a Kilauea olivine basalt, sample 654; three on a Hualalai ankaramite, sample C71; and two on a Hualalai alkali olivine basalt, sample C218). Results for olivine-liquid experiments conducted in air are also given in REUPDT but $K_{D,Fe^{+2}\text{-}Mg}$ for these experiments were ignored due to the extreme sensitivity of calculated values on phase composition.

Figure A1 shows the results of our MgO-based olivine and liquid mass balance calculations to produce, in combination with electron microprobe data, the molar FeO/MgO ratios in the experimental olivines and glasses. We use the same symbol set as Roeder and Emslie (1970) and a comparison of Fig. A1 with their Fig. 4 shows very good agreement in the distribution of points. The very subtle differences between the two figures likely reflect round-off errors and the different modes of plot generation. Our unweighted least-squares fit through the origin yields a slope (equal to $K_{D,Fe^{+2}\text{-}Mg}$) of 0.305 ± 0.005, in complete agreement with the value of 0.30 reported by Roeder and Emslie (1970). Considering the 27 individual $K_{D,Fe^{+2}\text{-}Mg}$ values, the overall range is from 0.26 to 0.36, almost all of which (0.27–0.36) is encompassed by the 22 olivine basalt experiments (composition 654). The mean and standard deviation for the entire data set is 0.31 ± 0.03 (the median value is also 0.31).

The individual $K_{D,Fe^{+2}\text{-}Mg}$ values based on MgO mass balance are not simply a random distribution of values with a large standard deviation as there is structure in the data associated with bulk composition, phase assemblage, and container material. In Fig. A2a, $K_{D,Fe^{+2}\text{-}Mg}$ is plotted in the form of a histogram and disaggregated according to the bulk composition. Experiments on the alkali olivine basalt (C218) and ankaramite bulk

compositions (C71) generally yield $K_{D,Fe^{+2}\text{-}Mg}$ values at the lower end of the distribution, except that $K_{D,Fe^{+2}\text{-}Mg}$ for 7-2-C71 is among the highest of the study. Similarly, $K_{D,Fe^{+2}\text{-}Mg}$ values for olivine ± trace spinel experiments are skewed to high values relative to the mean of all of the data (means of 0.33 vs. 0.30). We can't appeal to fractionation to dramatically alter liquid compositions from one experiment to the next because the calculated melt fractions are all greater than 0.87. Moreover, the bulk compositions are all similar, the range in SiO_2 and Na_2O+K_2O values being 47.9–49.4 and 2.6–3.3 wt % when each bulk composition is normalized to 100 wt %. Given the relatively small differences in glass compositions among the Roeder and Emslie (1970) experiments and literature data for basaltic melts, the large spread in $K_{D,Fe^{+2}\text{-}Mg}$ from 0.26–0.36 is surprising.

An additional type of systematic behavior can be seen when the $K_{D,Fe^{+2}\text{-}Mg}$ values are parsed by the experimental container material. For the most reducing conditions, Roeder and Emslie (1970) generally used alumina crucibles with the other experiments being conducted in either $Ag_{55}Pd_{45}$ or $Ag_{60}Pd_{40}$ alloy capsules. Figure A2b shows a histogram of $K_{D,Fe^{+2}\text{-}Mg}$ separated according to container material. $K_{D,Fe^{+2}\text{-}Mg}$ values obtained from the alumina crucible experiments form a coherent group ranging from 0.327–0.344 (0.337±0.008, mean and 1σ), whereas the Ag-Pd capsule runs display far greater variations (0.260–0.362; 0.303±0.026) that are not correlated with temperature or redox conditions. We conclude that we can reproduce Roeder and Emslie's (1970) calculations as they described them, but that the large scatter in the data, particularly among the Ag-Pd experiments, gives cause for concern. In the following two sections, we provide an independent critical assessment of the internal consistency of their data.

1.3. Some basic acceptance criteria for Roeder and Emslie's experiments

Before discussing the results of our mass balance calculations, we present some basic acceptance criteria as an initial quality check for the 27 experiments used by Roeder and Emslie (1970) to define $K_{D,Fe^{+2}\text{-}Mg}$. REUPDT gives full probe analyses of glass, excluding Cr_2O_3, but provides only wt % fayalite and forsterite for the olivine (2 digits), so that some of the usual tests of data quality for a crystalline phase, such as oxide totals or stoichiometry constraints, can't be used directly. We can, however, take advantage of

the low concentrations of elements other than Mg, Fe, and Si in olivine from basalts (e.g., Simkin and Smith, 1970; Sobolev e*t al*., 2007, and data therein). We accepted sums for olivine analyses between 97-103 but rejected run 8-2-C218 (wt % forsterite plus fayalite = 95) as requiring an implausible minor element contribution to bring the sum up to at least 97%. This run is excluded from any further consideration. Liquid compositions in terms of oxides also provide constraints on acceptable data. Oxide totals for probe analyses in REUPDT used to compute $K_{D,Fe^{+2}\text{-}Mg}$ range from 98.0 to 100.8 (computed with all Fe as FeO) and we accepted this range as being viable. The concentration of SiO_2 in glass from 7-8-654 is, however, anomalously high relative to other glass compositions from runs on the 654 bulk composition (Fig. A3) and we therefore rejected this experiment. A second experiment, 7-5-654, also has unusually high SiO_2 relative to other experiments whose glass compositions are shown in Fig. A3 but we retain it for the time being.

The REUPDT notes that two experiments, 7-1-654 and 9-1-654, contain clinopyroxene but there are no accompanying analyses. Clinopyroxene crystallization in basaltic magmas is often associated with major shifts in melt composition (e.g., Seaman *et al*., 2004) and we would be forced to reject these experiments if significant amounts of clinopyroxene were present because we would be unable to perform an accurate mass balance calculation. We therefore conducted a simple check for the onset of clinopyroxene crystallization by plotting CaO concentrations in the melt as a function of MgO, a variable sensitive to olivine fractionation (Fig. A4). Note that the open symbols (clinopyroxene present) in Fig. A4 are indistinguishable from values expected from a simple linear extension of the line calculated for the clinopyroxene-absent experiments. Had significant crystallization of clinopyroxene occurred, the open symbols would have plotted well below the line. We conclude that clinopyroxene crystallization can be neglected for these two experiments and have, therefore, included them in our subsequent analysis.

1.4. Mass balance calculations on Roeder and Emslie's (1970) data

Roeder and Emslie (1970) used MgO to mass balance olivine and glass so that they could determine $K_{D,Fe^{+2}\text{-}Mg}$. The major advantage to this approach is that it is not

computationally intensive, an important consideration in the 1960s. However, using only MgO also carries a major penalty because it neglects constraints on mass balance available through other elements. In this section, we consider the results of all phase (excluding clinopyroxene)-all oxide mass balance calculations as applied to REUPDT. We excluded two of Roeder and Emslie's 27 diagnostic experiments for reasons described above and performed mass balance calculations on the remaining 25, using the phase assemblage and compositions for each experiment as reported in REUPDT. As with our experiments, the mass balance calculations are based on a non-linear system of equations presented by Albarède and Provost (1977), which incorporates uncertainties on the bulk and phase compositions. Since most of Roeder and Emslie's experiments contained phases that weren't analyzed and some of the uncertainties are not given, we describe in the notes to Table A3 how we estimated required data not explicitly reported by Roeder and Emslie. For those experiments containing clinopyroxene, we assumed that the modal abundance was very small and could be neglected.

Modes, χ^2 values, sum of squared residuals, FeO and Fe_2O_3 in the melt, and $K_{D,Fe^{+2}\text{-}Mg}$ obtained from the full mass balance calculations for Roeder and Emslie's experiments are given in Table A3. Twenty-four of the 25 mass balance calculations yield χ^2 values between 0.2 and 8.4. All of these mass balance solutions are acceptable at the 95% confidence interval, i.e., the calculated *Q* value for the degrees of freedom associated with each mass balance calculation was ≥ 0.05, a consequence of the relatively large errors cited by Roeder and Emslie (1970). The χ^2 value for the mass balance fit of run 10-1-654 is, however, 29.6, yielding a *Q* of 0.00005 and we therefore rejected it from further consideration.

Calculated liquid abundances in the 24 provisionally accepted experiments range from 81.5 to 98.4 wt % with most or all of the balance being olivine. One experiment, 7-5-654, has anomalously low olivine (Fig. A5a) and high spinel (Fig. A5b) in the calculated mode relative to expectations based on the other 7-X-654 experiments (those conducted on the 654 bulk composition with $log\ fO_2 \sim -7$ and at variable temperatures). It also has high SiO_2 relative to other 654 experiments (Fig. A3) and the second highest discrepancy we observed between FeO* of the bulk composition as measured by electron microprobe of the completely fused starting material and FeO* for the bulk run product

obtained by wet chemistry (Table A3). It seems likely that a significant problem exists with this experiment and we therefore rejected it. Of the 27 experiments used by Roeder and Emslie (1970) to evaluate $K_{D,Fe^{+2}\text{-}Mg}$, we have thus far rejected four (8-2-C218 for low olivine sum, 7-8-654 for anomalously high SiO_2 in the glass, 7-5-654 for an inconsistent calculated mode, and 10-1-654 because of a poor fit in the mass balance calculation). For accepted experiments, the calculated olivine mode (Table A3) is between 1.4 and 12.2 wt %; when present, the spinel mode lies between 0.2 and 0.8 wt % and plagioclase abundances are < 6 wt %. As noted above, the clinopyroxene mode is assumed to be zero, even when present according to REUPDT.

In Fig. A6a, we compare calculated $K_{D,Fe^{+2}\text{-}Mg}$ values from our complete mass balance fits to those based solely on MgO, as used by Roeder and Emslie (1970). For individual experiments, $K_{D,Fe^{+2}\text{-}Mg}$ for the two calculation schemes differ by as much as 0.04 and MgO-based $K_{D,Fe^{+2}\text{-}Mg} > 0.32$ all convert to lower values in the full oxide mass balance calculations (but note that others are increased). Differences in $K_{D,Fe^{+2}\text{-}Mg}$ that are apparent in Fig. A6a are mostly a consequence of our using FeO* in the liquid as a mass balance constraint. For most experiments, the ratio of calculated $K_{D,Fe^{+2}\text{-}Mg}$ values is a linear function of ΔFeO* (liq), which we define as the percentage difference between (FeO + 0.89981 ×Fe_2O_3) in the liquid determined by mass balance and FeO* for the glass obtained using the electron microprobe (Fig. A6b; note that the liquid FeO and Fe_2O_3 contents determined by mass balance largely reflect the olivine FeO value and the wet chemistry bulk FeO and Fe_2O_3 values). In general, ΔFeO* (liq) > 0 leads to higher $K_{D,Fe^{+2}\text{-}Mg}$ values than expected from MgO-based mass balance and ΔFeO* (liq) < 0 leads to lower values. Overall, the all oxide-all phase mass balance yields a smaller standard deviation suggesting that some of the scatter in Roeder and Emslie's (1970) data is an artifact of their mass balance technique. The averages are nevertheless similar (0.312±0.027 for MgO-based mass balance versus 0.305±0.020) and systematic behaviors noted above in discussing Fig. A2 remain intact or are strengthened. For example, experiments conducted in Al_2O_3 crucibles yield a fairly tight cluster of $K_{D,Fe^{+2}\text{-}Mg}$ values (0.321±0.007) at the higher end of the distribution of all $K_{D,Fe^{+2}\text{-}Mg}$s whereas the Ag-Pd results are more scattered and generally lower (0.301±0.020). Similarly, data for the C71 and C218 bulk compositions are mostly at the low end of

calculated $K_{D,Fe^{+2}\text{-}Mg}$ values. Note that $K_{D,Fe^{+2}\text{-}Mg}$ for 7-2-C71, which is at the high end of $K_{D,Fe^{+2}\text{-}Mg}$ values when using MgO-based mass balance (0.343) becomes 0.301 and, mostly as a consequence of this, the average of the four C71 plus C218 experiments for an all-oxide all-phase mass balance calculation is lower, 0.28 instead of 0.30.

Figure A7 shows olivine-liquid $K_{D,Fe^{+2}\text{-}Mg}$ values calculated using all oxides and reported phases in REUPDT as a function of bulk ΔFeO*. There is no correlation between bulk ΔFeO* and $K_{D,Fe^{+2}\text{-}Mg}$ but we can distinguish three clusters of data, seven Ag-Pd experiments with bulk ΔFeO* < –3, two of which have bulk ΔFeO* < –5, a central region of five Al_2O_3 and eight Ag-Pd experiments with –3 < bulk ΔFeO* < +3, and four Ag-Pd experiments with bulk ΔFeO* > +3, three of which are > +5. Splits analyzed by wet chemistry are both Fe-enriched and Fe-depleted relative to the true bulk composition, consistent with wet chemistry splits being both crystal-enriched and crystal-depleted relative to the bulk composition. Variable amounts of Ag-Pd contamination in the analyzed splits may also play a role. We show below that there are questions concerning the quality of most of the data with very high or very low bulk ΔFeO* in Fig. A7.

The primary purpose of the mass balance calculations is to determine the FeO content of the melt so that $K_{D,Fe^{+2}\text{-}Mg}$ can be computed but it can also find use in testing for internal consistency. In the remainder of this section, we focus on the mass-balance generated Fe^{+3}/Fe^{+2} of the experimental glasses, because this allows us to more easily consider Roeder and Emslie's (1970) data in light of a large body of work on Fe^{+3}/Fe^{+2} values in melts as a function of temperature and fO_2.

For equilibrium between ferric and ferrous iron in a melt, the free energy of reaction for $FeO + 0.25\ O_2 = FeO_{3/2}$ can be expressed in the form

$$ln\left(\frac{X_{FeO_{3/2}}}{X_{FeO}}\right) = \frac{1}{4} ln\ f_{O_2} + \left[\frac{-G^{\circ}_{\rightarrow}}{RT} - ln\left(\frac{\gamma_{FeO_{3/2}}}{\gamma_{FeO}}\right)\right]$$

where $G^{\circ}_{\rightarrow}$, which is a function of temperature but not composition, is the standard state free energy of reaction and X_i and γ_i are the mole fraction and activity coefficient of *i*. If the last term on the right is independent of oxygen fugacity, then a plot of

$ln\left(X_{FeO_{3/2}}/X_{FeO}\right)$ at constant temperature against $lnfO_2$ will yield a slope of 0.25. In practice, $\gamma_{FeO_{3/2}}/\gamma_{FeO}$ is generally a function of composition and, therefore of fO_2, and thus the slope deviates from the ideal value of 0.25. Figure A8a shows an example for a basaltic liquid at 1200°C taken from data of Hill and Roeder (1974). An unweighted regression yields a slope of 0.20 and this is typical of results for basaltic liquids reported in the literature, which yield slopes of 0.19 to 0.23 (Fudali, 1965; Shibata, 1967; Hill and Roeder, 1974; Kress and Carmichael, 1988). Note that the slope in Fig. A8a is well defined and that all of the points are within ~2σ of the line. Note also that experiments in different container materials (alumina, Ag-Pd, and Pt) are all consistent with each other. We show below that consistency among the results of experiments produced in different container materials is an important issue for the data of Roeder and Emslie.

Figure A8b is a histogram compiling slopes for plots of $lnfO_2$ versus $ln\left(X_{FeO_{3/2}}/X_{FeO}\right)$ from literature experimental data and models for calculating Fe^{3+}/Fe^{2+}(see caption to Fig. A8 for references). We restrict attention to melts for which the experimental range in $lnfO_2$ exceeded 4.6 (i.e., 2 *log* units) because the scatter in best-fit slopes rose sharply when smaller ranges were considered. For simple systems, slopes ranged between 0.13 and 0.37 and for magmatic liquids, it was 0.19–0.23. We take the observed range for magmatic liquids, 0.19–0.23, to contain the expected value for Roeder and Emslie's liquids; values outside this range are problematic and any slope outside the range 0.13–0.37 can certainly be regarded as indicating a very serious problem. We use these criteria below to analyze the REUPDT for self-consistency.

Although run temperatures for the 23 provisionally accepted experiments in REUPDT range from 1152–1256, most of the data can be clustered into one of four groups, ~1153°C, ~1180°C, ~1200°C, and ~1225°C. There are four experiments conducted at higher temperatures (>1235°C), but the fO_2s are virtually identical, so we can't conduct an isothermal slope test for them. Figure A9 is a set of approximately isothermal plots of $lnfO_2$ versus $ln(Fe^{+3}/Fe^{+2})$ in order of ascending temperature. Figure A9a shows runs conducted in the vicinity of 1153°C. These are all experiments conducted in Ag-Pd capsules on bulk composition 654. An unweighted regression through the three points yields a slope of 0.32, which is well outside the expected range

for a basaltic liquid (0.19–0.23). It is not possible to construct a line with a viable slope using any pair of experiments involving the most ferric glass (7-1-654); the other two experiments, 8-1-654 and 9-1-654, do form a line with a viable slope (0.20), although the range in $lnfO_2$ is small (2.2 *ln* units). We conclude that 7-1-654 was compromised although the precise nature of the problem(s) is unclear. We tentatively accept 8-1-654 and 9-1-654. Fig. A9b shows a somewhat different case. Here, three Ag-Pd experiments generate a slope of 0.23, within the expected range, albeit via a very small range in $lnfO_2$ (2.5 *ln* units). The calculated slope for all four data points, one an Al_2O_3 experiment and three conducted in Ag-Pd capsules, is, however, 0.176 < 0.19, suggesting that either the Al_2O_3 datum is in error or that the alumina and Ag-Pd experiments are inconsistent with each other (e.g., if both sets are correct, then the Al_2O_3 and Ag-Pd data are on different lines). Since we can't distinguish between these possibilities based solely on this plot, we accept all of the data in Fig. A9b for the purposes of this test. Figure A9c shows a clearer inconsistency between the alumina and Ag-Pd experiments. The three Al_2O_3 experiments yield a slope of 0.19, within the expected range and, therefore, acceptable. A very different result is obtained for the five Ag-Pd experiments. Here the slope is 0.41, an implausibly high value. Deleting 6-1-654, the most ferric point, which is anomalous in Fig. A6b, does not lead to a viable line for the remaining Ag-Pd data (slope of 0.247). It is possible to draw a line sub parallel to the alumina data that goes through these lower four Ag-Pd data but this would imply that the alumina and Ag-Pd liquids have significantly different bulk compositions and that alumina addition to melts in the alumina experiments was very important in determining the Fe^{+3}/Fe^{+2} ratio (i.e., the bulk compositions are sufficiently different so that the data lie on different lines). This appears unlikely because the amount of alumina contamination in the alumina crucible experiments varies from experiment to experiment and yet all three points are consistent with the same line. Moreover, Fe^{+3}/Fe^{+2} models in the literature (e.g., Jayasuriya *et al*., 2004) show that Al is a modest driver of this ratio and we would therefore not expect the alumina and Ag-Pd experiments to produce significantly different lines. In addition, Hill and Roeder's (1974) data shown in Fig. A8a, which reflects experiments conducted in both alumina and Ag-Pd containers, are consistent with being on the same line. We conclude that some, if not all, of the ~1200°C Ag-Pd experiments reported in REUPDT

are in error and, since we can't distinguish reliably which, if any, might be valid, we reject all of them. For data obtained in the vicinity of 1225°C (Fig. A9d), the slope of 0.27 for the Ag-Pd data is higher than expectations for a basaltic melt (0.19–0.23) but, given the small range in $ln f O_2$ (2.3 *ln* units), we didn't enforce the slope consistency criterion for them. The alumina crucible experiment and the Ag-Pd data are consistent with a line whose slope is 0.18 (i.e., < 0.19). A higher slope could be obtained if the least ferric of the Ag-Pd experiments (7-6-654) were to be deleted or shifted in $ln f O_2$ but this would again be an arbitrary exercise and therefore, in the absence of additional data, we simply accepted all of the ~1225°C data. We conclude, based on Fig. A9, that the Al_2O_3 data can't be simultaneously consistent with all of the Ag-Pd data and that, even if one ignores the Al_2O_3 data, many of the Ag-Pd data are demonstrably inconsistent with expectations based on literature determinations of Fe^{+3}/Fe^{+2} at constant temperature. Where there is sufficient range in $ln f O_2$ to confidently determine the slope for Ag-Pd runs in an isothermal $ln f O_2$ vs. $ln(Fe^{+3}/Fe^{+2})$ plot (Figs. A9a and A9c), the data fail the slope test. Overall, we accepted twelve Ag-Pd experiments in the aftermath of the isothermal $ln f O_2$ vs. $ln(Fe^{+3}/Fe^{+2})$ slope test (two runs in Fig. A9a, three runs each shown in Figs. A9b and A9d and untested runs 7-2-C71 (1237°C), 7-10-654 (1238°C), 7-11-654 (1251°C) and 7-4-C71 (1266°C)) but it is important to note that this collection largely reflects insufficient data to apply the slope test for a given temperature and not a successful passage through it.

Figure A10, shows data for three ~1200°C alumina crucible experiments from REUPDT (Fig. 9c) together with the result for an additional basalt experiment, also run in an alumina crucible, reported by Hill and Roeder (1974). The slope based on all four experiments is 0.22, which is within the expected range. This result suggests that the alumina data of Roeder and Emslie (1970) are consistent with the alumina data of Hill and Roeder (1974). Since the alumina, Ag-Pd and Pt experiments of Hill and Roeder (1974) also yield a consistent Fe^{+3}/Fe^{+2} (Fig. A8a), this implies that the alumina crucible experiments of Roeder and Emslie (1970) are also consistent with the Ag-Pd experiments of Hill and Roeder (1974) and, therefore, the inconsistency of Roeder and Emslie's alumina and Ag-Pd data is not inherent to their use of these different container materials.

Our analysis through Fig. A9 was restricted to nearly isothermal sets of data but it is also possible to construct a test based on the temperature dependence of Fe^{+3}/Fe^{+2}. A wide variety of studies have demonstrated that $ln(Fe^{3+}/Fe^{2+})$ in an otherwise constant composition liquid is a linear function of inverse temperature but we are aware of only one determination for a magmatic liquid, a basalt studied by Kennedy (1948). Figure A11 is a histogram of the temperature dependence for Kennedy's basalt, a variety of simple systems, and models for magmatic liquids (see caption to Fig. A11 for references). Coefficients of $10^4/T(K)$ range from 0.7 to 2.5 but the range 0.7–1.4 captures Kennedy's basalt (1.04), all of the models for magmatic liquids (0.85–1.27), and all but three of the simple system determinations. We take the range of 0.7–1.4 as including the coefficient of $10^4/T(K)$ for all plausible basaltic liquids including those studied by Roeder and Emslie (1970).

A temperature dependence test can provide a constraint independent of the isothermal slope test because it can be used to test data from temperatures for which data are too sparse or too close in $ln fO_2$ to allow a testable isothermal slope to be determined. To correct Fe^{+3}/Fe^{+2} to some reference temperature $T_{ref}(K)$, we use the equation $ln(Fe^{+3}/Fe^{+2})$ at $T_{ref} = ln(Fe^{+3}/Fe^{+2})$ at $T_{exp} + C \times (10^4) \times (1/T_{ref} - 1/T_{exp})$, where T_{exp} refers to the run temperature and C is an empirical constant whose value is in the range 0.7–1.4 for Roeder and Emslie's liquids. The temperature test is essentially a special form of the isothermal slope test and it will be most sensitive when the difference between the experimental and reference temperature is maximized.

We selected a reference temperature of 1155°C for our variable temperature test because the highest temperature experiments were not tested using the isothermal slope test and because ~1155°C is the lowest temperature for which we conducted an isothermal test. In Fig. A12, we adjusted the Fe^{+3}/Fe^{+2} of the five alumina and twelve Ag-Pd experiments that provisionally passed all of the previously described tests to a reference temperature of 1155°C. Each point was weighted by the inverse of its variance in $ln(Fe^{+3}/Fe^{+2})$ and the value of C, the coefficient of $10^4/T(K)$ was allowed to float within the range 0.7–1.4 so that squared deviations of all points from the best-fit line were minimized. The resulting value of C is 0.94 and this is consistent to first order with the value of 1.04 obtained by Kennedy (1948) for a basalt. The temperature corrections

are relatively small, <0.36 *ln* units but noticeable, especially for the highest temperature data. If the data are all consistent with each other, we expect them to lie along a single line with a slope within the range 0.19–0.23 and since the best-fit line has a slope of 0.186, we regard this as a plausible result. Only two points (6-2-654 and, especially, 7-4-C71) lie much more than 2σ off the line and are, therefore, potential candidates for rejection and only one of these (7-4-C71) is outside the 95% confidence interval for placement of the line. However, we tentatively accept both.

As a final test, we again consider $K_{D,Fe^{+2}\text{-}Mg}$ as a function of bulk ΔFeO* (last shown in Fig. A7), but now plot only the data that passed all of our previous tests (Fig. A13). Upon comparing Figs. A7 and A13, it is immediately apparent that the Ag-Pd experiments at bulk ΔFeO* > +3 observed in Fig. A7 have disappeared, except for 7-1-C218 (bulk ΔFeO* = +6.7), and that, although there are still several experiments with bulk ΔFeO* < –3, only one of these, 7-4-C71 (bulk ΔFeO* = –8.5), is below –5. We note that 7-4-C71 is also anomalous in Fig. A12. Given the natural gaps between the central cluster at –5 < bulk ΔFeO* < +3 and the two anomalous points and the fact that all of the other data with similarly large deviations in bulk ΔFeO* from zero can be shown to be compromised, we reject both 7-4-C71 and 7-1-C218.

1.5. Discussion

Overall, 15 of 27 experiments used by Roeder and Emslie (1970) pass all of our quality filters giving us an accepted collection of experiments to interrogate for $K_{D,Fe^{+2}\text{-}Mg}$ values and, finally, to address the issue of what Roeder and Emslie's data imply for $K_{D,Fe^{+2}\text{-}Mg}$. For the alumina crucible experiments, we obtain $K_{D,Fe^{+2}\text{-}Mg}$ of 0.321±0.007. For accepted Ag-Pd experiments, we find $K_{D,Fe^{+2}\text{-}Mg}$ of 0.306±0.011 and, for the entire data set, we obtain $K_{D,Fe^{+2}\text{-}Mg}$ of 0.311±0.012. Note that our analysis of Roeder and Emslie's data has reduced the scatter for the entire data set relative to that of the original ($K_{D,Fe^{+2}\text{-}Mg}$ = 0.312±0.027) but the means are virtually identical. It is also noteworthy that, although our inferred means for Roeder and Emslie's data are low relative to the 0.345±0.009 we obtained for our data and the 0.340±0.012 for literature data on broadly tholeiitic compositions, all of these estimates overlap at 2σ.

At first glance, it would seem that we have expended considerable effort to end up in essentially the same place as Roeder and Emslie (1970). The canonical value for $K_{D,Fe^{+2}\text{-}Mg}$ is 0.30 (cf. Fig. A1) and the average for their individual experiments is 0.31. Our average for all accepted experiments from REUPDT is 0.31 (0.32 if the alumina experiments are preferred), which is lower than the ~0.34 we obtained and we are, therefore, left with a gap of 0.02–0.03 in $K_{D,Fe^{+2}\text{-}Mg}$. In Fig. A14, we show a sensitivity diagram for a typical run with 8.2 wt % FeO in the melt and $K_{D,Fe^{+2}\text{-}Mg} = 0.30$. The wet chemical determination of FeO in a bulk run product can significantly affect $K_{D,Fe^{+2}\text{-}Mg}$ and if a FeO determination was 10% high, this could explain a $K_{D,Fe^{+2}\text{-}Mg}$ difference of 0.03. However, bulk ΔFeO* deviations of accepted data (–5 to +3 %; Fig. A13) limit possible systematic errors in bulk FeO such that this source is unlikely to shift $K_{D,Fe^{+2}\text{-}Mg}$ by no more than a few hundredths. Systematic microprobe errors can also significantly affect $K_{D,Fe^{+2}\text{-}Mg}$, and it is important to remember that a microprobe in the late 60s was a very different instrument than we have today. A clear indication of this can be seen in the fact that Roeder and Emslie used working curves to obtain quantitative compositional information and it is possible that this led to systematic errors. If, for example, their fayalite numbers were low relative to forsterite by just 1 on average, their inferred $K_{D,Fe^{+2}\text{-}Mg}$ would be low by ~0.02 (Fig. A14); we note that the olivine totals (Fa + Fo) in REUPDT are generally low. Similarly, if MgO concentrations in the liquid from REUPDT are low by 2σ, this would shift $K_{D,Fe^{+2}\text{-}Mg}$ up by ~0.03. Roeder and Emslie (1970) note that their errors are probably overstated, so that the nominal 2σ MgO effect shown in Fig. A14 may well refer to more than 2σ, but the point remains that systematic errors in glass composition can account for substantial differences in $K_{D,Fe^{+2}\text{-}Mg}$.

Finally, it is worth considering what the average $K_{D,Fe^{+2}\text{-}Mg}$ value would be using the individual MgO-based $K_{D,Fe^{+2}\text{-}Mg}$s and our collection of "accepted" experiments, i.e., what might Roeder and Emslie have reported as the average olivine-liquid $K_{D,Fe^{+2}\text{-}Mg}$ given this set of experiments. The average $K_{D,Fe^{+2}\text{-}Mg}$ value (both alumina and Ag-Pd experiments) using MgO-based mass balance calculations on olivine and liquid would have been 0.315±0.021, higher than the canonical 0.30 and within error of the 0.34 we inferred in this work. As was the case with the full data set, the alumina experiments

yield $K_{D,Fe^{+2}\text{-}Mg}$s that define a tight cluster (mean = 0.336±0.008, 1σ), whereas the remaining Ag-Pd experiments vary from a high of 0.34 to a low of 0.28, with a mean of 0.305±0.017 (virtually identical to the canonical value). Note that accepting the alumina data yields an average olivine-liquid $K_{D,Fe^{+2}\text{-}Mg}$ that is essentially identical to the one obtained in our work.

1.6. Concluding thoughts

Finally, it is important to put our analysis of Roeder and Emslie's data in its proper place. The essence of Roeder and Emslie (1970) is not to be found in any specific value of $K_{D,Fe^{+2}\text{-}Mg}$. Nor is it in the efficacy of any particular experiment or collection of experiments. It is in the realization that an experimental study of crystal-liquid partitioning in a complex system can yield quantitative insights into the origin and evolution of natural magmatic liquids. It is in the realization that modern analytical techniques are tools that can provide great insight into igneous processes, especially if supported quantitatively through experimentation. It is in the motivation provided to many hundreds of later researchers, some of whom took the basic concepts of Roeder and Emslie and transformed them into new but related ways of looking at geological problems. These are the true legacies of Roeder and Emslie and there is nothing here that can or should affect them.

2. Projection of Olivine-Liquid Exchange Coefficients

In this section, we expand on the brief summary given in the main text of the projection scheme we used to reduce the dependence of olivine-liquid $K_{D,Fe^{+2}\text{-}Mg}$ on the phase compositions.

We begin by computing molar CMAS components of the liquid as defined by the projection scheme used in BVSP (1981, chapter 3.3):

$$C = (CaO - P_2O_5/3 + K_2O + Na_2O) \quad \text{(A1a)}$$

$$M = (MgO + FeO + MnO) \quad \text{(A1b)}$$

$$A = (Al_2O_3 + Cr_2O_3 + Fe_2O_3 + Na_2O) \quad \text{(A1c)}$$

$$S = SiO_2 - 2\times Na_2O - 4\times K_2O), \quad \text{(A1d)}$$

where the oxides are on a molar basis (e.g., mole % or mole fractions). The value of "S" as used here and in the main article is then defined as

$$\text{"S"} = S/(C + M + A + S). \quad \text{(A1e)}$$

Figure A15a shows values of $K_{D,Fe^{+2}\text{-}Mg}$ vs. "S" for our nine QFM experiments (Table 3) and a collection of 446 experimentally determined olivine-liquid pairs obtained at QFM±0.25 taken from the literature (see section 4 for references to the data used). Values of FeO/Fe_2O_3 in the liquids for this figure were calculated using eqn 12 of Jarasuriya *et al*. (2004), one of the several available Fe^{2+}/Fe^{3+} algorithms discussed in the main text. The solid black curve is an unweighted least-squares fit to the equation:

$$K_{D,Fe^{+2}\text{-}Mg} = a + b\times\exp(c\times\text{"S"}), \quad \text{(A2)}$$

for all of the data, where a (0.4523), b (–0.5372), and c (–3.2001) are the least-squares fit parameters. To obtain the projection of an experimentally determined value of $K_{D,Fe^{+2}\text{-}Mg}$ to a value of "S" = 0.5, we project along a curve parallel to the global fit, i.e.,

$$[K_{D,Fe^{+2}\text{-}Mg}]_{0.5} = K_{D,Fe^{+2}\text{-}Mg} - [a + b\times\exp(c\times\text{"S"})] + [a + b\times\exp(c\times 0.5)] \quad \text{(A3)}$$

where "S" in the equation above is the value of "S" associated with the particular $K_{D,Fe^{+2}\text{-}Mg}$ value being projected. Two sample projection paths are shown schematically as red curves in Fig. A15a for experimentally determined points with "S" = 0.3994 (i.e., experimental "S" <0.5) and the other with an experimental "S" = 0.5508 (i.e., experimental "S" >0.5; both points are plotted as larger open circles).

The purpose of this initial projection (eqns A1–A3; Fig. A15a) is to remove first order effects of the liquid composition on $K_{D,Fe^{+2}\text{-}Mg}$. These projected data points are, however, correlated with the experimentally determined Fo contents of the olivine as

shown in Fig. A15b. This suggests a dependence of $K_{D,Fe^{+2}\text{-}Mg}$ on the olivine composition, a point discussed by Toplis (2005) and Tuff and O'Neill (2010), and thus we can use the olivine composition to construct a second projection. We begin by defining a global unweighted linear least-squares fit to our QFM±0.25 database (black line in Fig. A15b):

$$[K_{D,Fe^{+2}\text{-}Mg}]_{0.5} = d + e \times [Mg/(Mg+Fe)]^{ol} \quad (A4)$$

where d (0.4045) and e (0.07799) are least-squares fit parameters. Individual data points are then projected to Fo_{88}:

$$[K_{D,Fe^{+2}\text{-}Mg}]_{0.5,88} = [K_{D,Fe^{+2}\text{-}Mg}]_{0.5} - \{d + e \times [Mg/(Mg+Fe)]^{ol}\} + \{d + e \times [0.88]^{ol}\} \quad (A5)$$

This is shown schematically in Fig. A15b for two points shown as larger open blue circles (the same two points that are plotted as larger open black circles in panel a). Red lines extend from these two points parallel to the global fit to the open gray circles at an olivine Mg/(Mg+Fe) value of 0.88. Projecting the solid blue circles parallel to the least-squares line These doubly projected points appear in histogram form in Fig. 4 of the main article.

Figure A16 compares unprojected $K_{D,Fe^{+2}\text{-}Mg}$ values from the QFM±0.25 data set to the doubly-projected $K_{D,Fe^{+2}\text{-}Mg}$s. Although the mean values of the two data sets are very similar, projecting the $K_{D,Fe^{+2}\text{-}Mg}$s to "S" = 0.5 and Fo_{88} has decreased the standard deviation by a factor of two and removed essentially all of the skewness apparent in the distribution in Fig. A16a. In our view this makes it much easier to visually compare histograms of $K_{D,Fe^{+2}\text{-}Mg}$s that have been calculated using different Fe^{+3}/Fe^{+2} algorithms.

3. Comparisons of Our Data with predictions of the Models of Ford *et al.* (1983) and Toplis (2005)

Ford *et al*. (1983) and Toplis (2005) parameterized Fe^{+2}-Mg partitioning between olivine and melt based on large numbers of 1-atm and high-pressure experiments. Both

parameterizations have been used in olivine-addition calculations where the goal is to estimate the compositions of parental mantle melts (e.g., Herzberg *et al*., 2007; Putirka *et al*., 2007) but both models predict substantially lower $K_{D,Fe^{+2}-Mg}$ values than we obtain for our QFM and NNO experiments and of the QFM±0.25 data set from the literature if Jayasuriya *et al*. (2004) equation 12 is used to compute Fe^{+3}/Fe^{+2} in the melt. In this section, we examine the causes of differences between predictions of the Ford *et al*. and Toplis models and observed and calculated results for our experiments and those from the literature.

Both the Ford *et al*. (1983) and Toplis (2005) models depend critically on the Fe^{+3}/Fe^{+2} algorithm used to calculate FeO in the liquid as this is required to calculate $K_{D,Fe^{+2}-Mg}$. Consider first Ford *et al*. (1983), who used the equation presented by Sack *et al*. (1980). $K_{D,Fe^{+2}-Mg}$ values calculated using Sack *et al*. (1980) to obtain Fe^{+3}/Fe^{+2} in the liquid for the QFM±0.25 data set are 0.014±0.008 lower than they are if eqn 12 of Jayasuriya *et al*. (2004) is used with differences ranging between –0.014 (i.e., using Sack *et al*. yields a higher $K_{D,Fe^{+2}-Mg}$) and +0.041. Thus, the Ford *et al*. expression will on average predict $K_{D,Fe^{+2}-Mg}$s for liquids at fO_2s near QFM that are ~0.014 lower than those preferred here due solely to the different choice of Fe^{+3}/Fe^{+2} algorithm. However, we obtain a larger difference if we apply either the Sack *et al*. (1980) Fe^{+3}/Fe^{+2} algorithm or the $K_{D,Fe^{+2}-Mg}$ expression of Ford *et al*. (1983) to our QFM experiments. If we calculate $K_{D,Fe^{+2}-Mg}$ using the Fe^{+3}/Fe^{+2} expression of Sack *et al*. (1980), we obtain 0.320±0.009. The model of Ford *et al*. (1983) gives 0.318±0.009. These calculations are in good agreement with each other but are 0.023 and 0.025 lower (not ~0.014) than the mean $K_{D,Fe^{+2}-Mg}$ calculated for the same runs (0.343±0.008) using the wet chemistry FeO value for run # 26 and eqn 12 of Jayasuriya *et al*. (2004) for the remaining experiments. For run # 26 (1500°C, QFM), the deviation is even larger. A $K_{D,Fe^{+2}-Mg}$ value of 0.338±0.005 is observed experimentally for our run #26 (QFM, 1500°C) and, since Fe^{+3}/Fe^{+2} was determined through wet chemistry, it is independent of Fe^{+3}/Fe^{+2}

algorithm. This $K_{D,Fe^{+2}-Mg}$ value is 0.034 higher than the 0.304 predicted by the Ford *et al*. model, well outside the 0.014±0.008 expected based on the literature QFM±0.25 data set. The discrepancies we have just described with respect to model predictions for our data are closely tied to the temperature dependence of Ford *et al*.'s (1983) model as the deviations generally increase with increasing temperature (Fig. A17). This effect appears to be driven primarily by the temperature dependence of Fe^{+3}/Fe^{+2} as calculated by Sack *et al*. (1980) relative to that calculated by Jayasuriya *et al*. (2004), as shown in Fig. A18. This different temperature dependence is propagated through the Ford *et al*. (1983) model, which uses Sack *et al*. (1980), to yield low $K_{D,Fe^{+2}-Mg}$ values at high temperatures (or high MgO contents) and suggests that the Ford *et al*. (1983) $K_{D,Fe^{+2}-Mg}$ model is inaccurate for the highly magnesian liquids relevant to parental melts.

We can perform a similar analysis using the Toplis (2005) model to calculate $K_{D,Fe^{+2}-Mg}$. Toplis (2005) incorporates the Fe^{+3}/Fe^{+2} expression of Kilinc *et al*. (1983) into his model with an additional term for P_2O_5 taken from Toplis *et al*. (1994). For the QFM±0.25 data set from the literature, the Kilinc *et al*. (1983) model yields $K_{D,Fe^{+2}-Mg}$ values that are 0.015±0.007 lower than those generated using Jayasuriya *et al*. (2004). This is similar to our observations described above for the Sack *et al*. (1980) Fe^{+3}/Fe^{+2} model. The mean $K_{D,Fe^{+2}-Mg}$ value for our QFM data calculated using the model of Toplis (2005) is 0.313±0.009, 0.030 lower than our mean $K_{D,Fe^{+2}-Mg}$ value of 0.343±0.008 (i.e., this is twice the deviation expected based solely on the different calculation schemes for Fe^{+3}/Fe^{+2}). In contrast to the Sack *et al.* (1980) model described above, there is no substantive and systematic temperature difference in the Kilinc *et al*. (1983) model for Fe^{+3}/Fe^{+2} relative to Jayasuriya *et al*. (2004) and yet there is a clear temperature dependence implicit in Fig. A17 for $K_{D,Fe^{+2}-Mg}$ values calculated using the Toplis (2005) model. A possible source for the unexpectedly large deviations and temperature dependence is the use of high-pressure olivine-liquid data in parameterizing equations for $K_{D,Fe^{+2}-Mg}$. Such data extends to significantly higher temperatures than the

1-atm data set (Fig. A19) so that values for temperature and pressure coefficients are likely to be dominated by these data and, since pressure and temperature are correlated for these experiments, the coefficients are also likely to be correlated. Also, since the high pressure data used by Toplis (2005) include experiments run in Re (probably quite oxidizing), graphite (oxidizing enough to require a correction for the presence of Fe^{+3}) and iron (probably reducing enough not to require a correction for Fe^{+3}), there are likely to be trade-offs among the coefficients of temperature, pressure, and chemical terms to compensate for variable Fe^{+3}/Fe^{+2} ratios that are not taken into account. Refitting the model of Toplis (2005) to establish the influences of specific data on the coefficients is beyond the scope of this study but, as noted in the main text, neglecting Fe^{+3} in the melt for high pressure graphite experiments leads to low estimates of $K_{D,Fe^{+2}-Mg}$, which would be consistent with the Toplis (2005) model underestimating $K_{D,Fe^{+2}-Mg}$ values for our experiments (Fig. A17) and, by extension, $K_{D,Fe^{+2}-Mg}$ values for high-temperature, magnesian parental melts.

References for Sections 1 - 3:

Albarède, F. & Provost, A. (1977). Petrological and geochemical mass-balance equations: an algorithm for least-square fitting and general error analysis. *Computers and Geosciences* **3**, 309–326.

Ariskin, A. A. & Barmina, G. S. (1999). An empirical model for the calculation of spinel-melt equilibria in mafic igneous systems at atmospheric pressure: 2. Fe-Ti oxides. *Contributions to Mineralogy and Petrology* **134**, 251–263.

Beattie, P. (1993). Olivine-melt and orthopyroxene-melt equilibria. *Contributions to Mineralogy and Petrology* **115**, 103-111.

Beattie, P., Ford, C. & Russell, D. (1991). Partition coefficients for olivine-melt and orthopyroxene-melt systems. *Contributions to Mineralogy and Petrology* **109**, 212–224.

Borisov, A. A. & Shapkin, A. I. (1989). New empirical equation of dependence of Fe^{3+}/Fe^{2+} ratio in natural melts on their composition, oxygen fugacity and temperature. *Geokhimiya* **1989**, (6), 892–897 [*Geochemistry International* (1989) **27** (1), 111–116].

Bowker, J. C., Lupis, C. H. P. & Flinns, P. A. (1981). Structural studies of slags by Mössbauer spectroscopy. *Canadian Metallurgical Quarterly* **20**, 69–78.

BVSP (1981) *Basaltic Volcanism on the Terrestrial Planets*. New York: Pergamon Press.

Dingwell, D. B. & Virgo, D. (1987). The effect of oxidation sate on the viscosity of melts in the system Na_2O-FeO-Fe_2O_3-SiO_2. *Geochimica et Cosmochimica Acta* **51**, 195–205.

Ford, C. E., Russell, D. G., Craven, J. A. & Fisk, M. R. (1983). Olivine-liquid equilibria: Temperature, pressure and composition dependence of the crystal/liquid cation partition coefficients for Mg, Fe^{2+}, Ca and Mn. *Journal of Petrology* **24**, 256–265.

Fudali, R. F. (1965). Oxygen fugacities of basaltic and andesitic magmas. *Geochimica et Cosmochimica Acta* **29**, 1063–1075.

Ghiorso, M. S. & Kress, V. C. (2004). An equation of state for silicate melts. II. Calibration of volumetric properties at 10^5 Pa. *American Journal of Science* **304**, 679–751.

Herzberg, C., Asimow, P. D., Arndt, N., Niu, Y., Lesher, C. M., Fitton, J. G., Cheadle, M. J. & Saunders, A. D. (2007). Temperatures in ambient mantle and plumes: Constraints from basalts, picrites, and komatiites. *Geochemistry Geophysics Geosystems* **8**, Q02006, doi:10.1029/2006GC001390.

Hill, R. & Roeder, P. (1974). The crystallization of spinel from basaltic liquid as a function of oxygen fugacity. *Journal of Geology* **82**, 709–729.

Iwase, M., Okumura, T., Kawamura, K., Miyamoto, Y. & Oh-uchi, H. (1998). Oxidation-reduction equilibrium of Fe^{3+}/Fe^{2+} in a candidate glass for immobilisation of high level nuclear waste. *Glass Technology* **39**, 142–146.

Jayasuriya, K. D., O'Neill,H. St. C., Berry, A. J. & Campbell, S. J. (2004). A Mössbauer study of the oxidation state of Fe in silicate melts. *American Mineralogist* **89**, 1597–609.

Johnston, W. D. (1964). Oxidation-reduction equilibria in iron-containing glass. *Journal of the American Ceramic Society* **47**, 198–201.

Kennedy, G. C. (1948). Equilibrium between volatiles and iron oxides in igneous rocks. *American Journal of Science* **246**, 529–549.

Kilinc, A., Carmichael, I. S. E., Rivers, M. L. & Sack, R. O. (1983). The ferric-ferrous ratio of natural silicate liquids equilibrated in air. *Contributions to Mineralogy and Petrology* **83**, 136–140.

Kress, V. C. & Carmichael, I. S. E. (1988). Stoichiometry of the iron oxidation reaction in silicate melts. *American Mineralogist* **73**, 1267–1274.

Kress, V. C. & Carmichael, I. S. E. (1989). The lime-iron-silicate melt system: Redox and volume systematics. *Geochimica et Cosmochimica Acta* **53**, 2883–2892.

Kress, V. C. & Carmichael, I. S. E. (1991). The compressibility of silicate liquids containing Fe_2O_3 and the effect of composition, temperature, oxygen fugacity and pressure on their redox states. *Contributions to Mineralogy and Petrology* **108**, 82–92.

Lange, R. A. & Carmichael, I. S. E. (1989). Ferric-ferrous equilibria in Na_2O-FeO-Fe_2O_3-SiO_2 melts: Effects of analytical techniques on derived partial molar volumes. *Geochimica et Cosmochimica Acta* **53**, 2195–2204.

Larson, H. & Chipman, J. (1953). Oxygen activity in iron oxide slags. *Transactions of the American Institute of Mining and Metallurgical Engineers* **197**, 1089–1096.

Libourel, G. (1999). Systematics of calcium partitioning between olivine and silicate melt: implications for melt structure and calcium content of magmatic olivines. *Contributions to Mineralogy and Petrology* **136**, 63-80.

Mysen, B. O. & Virgo, D. (1983). Redox equilibria, structure, and melt properties in the system Na_2O-Al_2O_3-SiO_2-Fe-O. *Carnegie Institution of Washington Yearbook* **82**, 313–317.

Mysen, B. O., Virgo, D., & Seifert, F. A. (1984). Redox equilibria of iron in alkaline earth silicate melts: relationships between melt structure, oxygen fugacity, temperature and properties of iron-bearing silicate liquids. *American Mineralogist* **69**, 834–847.

Mysen, B. O., Virgo, D., Neamann, E. G. & Seifert, F. A. (1985a). Redox equilibria and the structural states of ferric and ferrous iron in melts in the system CaO-MgO-Al_2O_3-SiO_2-Fe-O: relationships between redox equilibria, melt structure and liquidus phase equilibria. *American Mineralogist* **70**, 317–331.

Mysen, B. O., Virgo, D., Scarfe, C. M. & Cronin, D. J. (1985b). Viscosity and structure of iron- and aluminum-bearing calcium silicate melts at 1 atm. *American Mineralogist* **70**, 487–498.

Nikolaev, G. S., Borisov, A. A. & Ariskin, A. A. (1996). Calculation of ferric-ferrous ratio in magmatic melts: Testing and additional calibration of empirical equations for various magmatic series. *Geokhimiya* **1996**, (8), 713–722 [*Geochemistry International* (1996) **34** (8), 641–649].

Ohashi, S., Kashimura, N., Uchida, Y., McLean, A. & Iwase, N. (2000). Oxidation-reduction equilibria of ferrous/ferric ions in oxide melts. *Steel Research* **71**, 375–380.

O'Horo, M. P. & Levy, R. A. (1978). Effect of melt atmosphere on the magnetic properties of a $[(SiO_2)_{45}(CaO)_{55}]_{65}[Fe_2O_3]_{35}$ glass. *Journal of Applied Physics* **49**, 1635–1637.

O'Neill, H. St. C. (1987). Quartz-fayalite-iron and quartz-fayalite-magnetite equilibria and the free energy of formation of fayalite (Fe_2SiO_4) and magnetite (Fe_3O_4). *American Mineralogist* **72**, 67–75.

Poustovetov, A. A. & Roeder, P. L. (2001). Numerical modeling of major element distribution between chromian spinel and basaltic melt, with application to chromian spinel in MORBs. *Contributions to Mineralogy and Petrology* **142**, 58–71.

Putirka, K. (2005). Igneous thermometers and barometers based on plagioclase plus liquid equilibria: Tests of some existing models and new calibrations. *American Mineralogist* **90**, 336-346.

Putirka, K. D., Perfit, M., Ryerson, F. J. & Jackson, M. G. (2007). Ambient and excess mantle temperatures, olivine thermometry, and active vs. passive upwelling. *Chemical Geology* **241**, 177–206.

Rhodes, J. M. (1996). Geochemical stratigraphy of lava flows sampled by the Hawaii Scientific Drilling Project. *Journal of Geophysical Research* **101**, 11729-11746.

Rhodes, J. M. & Vollinger. M. J. (2004). Composition of basaltic lavas sampled by phase-2 of the Hawaii Scientific Drilling Project: Geochemical stratigraphy and magma types. *Geochemistry, Geophysics, Geosystems* **5**, Q07G13, doi:10.1029/2002GC000434.

Roeder, P. L. & Emslie, R. F. (1970). Olivine-liquid equilibrium. *Contributions to Mineralogy and Petrology* **29**, 275–289.

Sack, R. O., Carmichael, I. S. E., Rivers, M. & Ghiorso, M.S. (1980). Ferric-ferrous equilibria in natural silicate liquids at 1bar. *Contributions to Mineralogy and Petrology* **75**, 369–376.

Schreiber, H. D., Lauer, H. V. & Thanyasiri, T. (1980). The redox state of cerium in basaltic magmas: an experimental study of iron-cerium interactions in silicate melts. *Geochimica et Cosmochimica Acta* **44**, 1599–1612.

Schreiber, H. D., Kozak, S. J., Merkel, R.C., Balazs, G.B. & Jones, P.W. (1986). Redox equilibria and kinetics of iron in a borosilicate glass-forming melt. *Journal of Non-Crystalline Solids* **84**, 186–195.

Seaman, C., Sherman, S. B., Garcia, M.O., Baker, M.B., Balta, B. & Stolper, E. (2004). Volatiles in glasses from the HSDP2 drill core. *Geochemistry Geophysics Geosystems* **5**, Q09G16, doi:10.1029/2003GC000596, 42 pp.

Shibata, K. (1967). The oxygen pressure of the magma from Mihara volcano, O-sima, Japan. *Bulletin of the Chemical Society of Japan* **40**, 830–834.

Simkin, T. & Smith, J. V. (1970). Minor-element distribution in olivine. *Journal of Geology* **78**, 304–325.

Sobolev, A. V., Hofmann, A. W., *et al.* (2007). The amount of recycled crust in sources of mantle-derived melts. *Science* **316**, 412–417.

Stolper, E., Sherman, S., Garcia, M., Baker, M. & Seaman, C. (2004). Glass in the submarine section of the HSDP2 drill core, Hilo, Hawaii. *Geochemistry, Geophysics, Geosystems* **5**, Q07G15, doi:10.1029/2003GC000553.

Timucin, M. & Morris, A. E. (1970). Phase equilibria and thermodynamic studies in the system CaO-FeO-Fe_2O_3-SiO_2. *Metallurgical Transactions* **1**, 3193–3201.

Toplis, M. J. (2005). The thermodynamics of iron and magnesium partitioning between olivine and liquid: criteria for assessing and predicting equilibrium in natural and experimental systems. *Contributions to Mineralogy and Petrology* **149**, 22–39.

Toplis, M. J., Dingwell, D. B. & Libourel, G. (1994). The effect of phosphorus on the iron redox ratio, viscosity, and density of an evolved ferro-basalt. *Contributions to Mineralogy and Petrology* **117**, 293–304.

Tsuchiyama, A., Nagahara, H. & Kushiro, I. (1981). Volatilization of sodium from silicate melt spheres and its application to the formation of chondrules. *Geochimica et Cosmochimica Acta* **45**, 1357–1367.

Tuff, J. & O'Neill, H. St. C. (2010). The effect of sulfur on the partitioning of Ni and other first-row transition elements between olivine and silicate melt. *Geochimica et Cosmochimica Acta* **74**, 6180–6205.

Virgo, D., Mysen, B. O. & Danckwerth, P. (1983). The coordination of Fe^{3+} in oxidized vs. reduced sodium aluminosilicate glasses: ^{57}Fe Mössbauer study. *Carnegie Institution of Washington Yearbook* **82**, 309–313.

4. Experimental Database References

In addition to data from this work, we drew from the following literature sources for olivine-liquid pairs. Criteria for data selection are discussed in the main text.

Agee, C. B. & Walker, D. (1990). Aluminum partitioning between olivine and ultrabasic silicate liquid to 6 GPa. *Contributions to Mineralogy and Petrology* **105**, 243–254.

Akella, J., Williams, R. J. & Mullins, O. (1976). Solubility of Cr, Ti, and Al in co-existing olivine, spinel, and liquid at 1 atm. *Proceedings of the Seventh Lunar Science Conference*, 1179–1194.

Auwera, J. V. & Longhi, J. (1994). Experimental study of the jotunite (hypersthene monzodiorite): constraints on the parent magma composition and crystallization conditions (P,T, fO_2) of the Bjerkreim-Sokndal layered intrusion (Norway). *Contributions to Mineralogy and Petrology* **118**, 60–78.

Baker, M. B., Grove, T. L. & Price, R. (1994). Primitive basalts and andesites from the Mt. Shasta region, N. California: products of varying melt fraction and water content. *Contributions to Mineralogy and Petrology* **118**, 111–129.

Bartels, K. S. & Furman, T. (2002). Effect of sonic and ultrasonic frequencies on the crystallization of basalt. *American Mineralogist* **87**, 217–226.

Bartels, K. S. & Grove, T. L. (1991). High-pressure experiments on magnesian eucrite compositions: Constraints on magmatic processes in the eucrite parent body. *Proceedings of the Lunar and Planetary Science Conference* **21**, 351–365.

Bartels, K. S., Kinzler, R. J. & Grove, T. L. (1991). High pressure phase relations of primitive high-alumina basalts from Medicine Lake volcano, northern California. *Contributions to Mineralogy and Petrology* **108**, 253–270.

Bickle, M. J. (1978). Melting experiments on peridotitic komatiites. In: W. S. MacKenzie (ed.)*Progress in experimental petrology; fourth progress report of research supported by N.E.R.C., 1975–1978*. pp. 187–195. Natural Environment Research Council: London, United Kingdom.

Brophy, J. G. (1995). 1-atm melting study of a Leg 142 basalt: implications for fractionation processes beneath the East Pacific Rise at 9°30'N. *Proceedings of the Ocean Drilling Program, Scientific Results* **142**, 41–49.

Delano, J. W. (1977). Experimental melting relations of 63545, 76015, and 76055 *Proceedings of the Eighth Lunar Science Conference*, 2097–2123.

Delano, J. W. (1980). Chemistry and liquidus phase relations of Apollo 15 red glass: Implications for the deep lunar interior. *Proceedings of the Eleventh Lunar and Planetary Science Conference*, 251–288.

Donaldson, C. H., Usselman, T. M., Williams, R. J. & Lofgren, G. E. (1975). Experimental modeling of the cooling history of Apollo 12 olivine basalts. *Proceedings of the Sixth Lunar Science Conference*, 843–869.

Draper, D. S. & Johnston, A. D. (1992). Anhydrous PT phase relations of an Aleutian high-MgO basalt: an investigation of the role of olivine-liquid reaction in the generation of arc high-alumina basalts. *Contributions to Mineralogy and Petrology* **112**, 501–519.

Dunn, T. & Sen, C. (1994). Mineral/matrix partition coefficients for orthopyroxene, plagioclase, and olivine in basaltic to andesitic systems: A combined analytical and experimental study. *Geochimica et Cosmochimica Acta* **58**, 717–733.

Dunn, T. & Stringer, P. (1990). Petrology and petrogenesis of the Ministers Island dike, southwest New Brunswick, Canada. *Contributions to Mineralogy and Petrology* **105**, 55–65.

Ehlers, K., Grove, T. L., Sisson, T. W., Recca, S. I. & Zervas, D. A. (1992). The effect of oxygen fugacity on the partitioning of nickel and cobalt between olivine, silicate melt, and metal. *Geochimica et Cosmochimica Acta* **56**, 3733–3743.

Gaetani, G. A., Grove, T. L. & Bryan, W. B. (1994). Experimental phase relations of basaltic andesites from hole 839B under hydrous and anhydrous conditions. *Proceedings of the Ocean Drilling Program, Scientific Results* **135**, 557–563.

Gee, L. L. & Sack, R. O. (1988). Experimental petrology of melilite nephelinites. *Journal of Petrology* **29**, 1233–1255.

Grove, T. L. (1981). Use of FePt alloys to eliminate the iron loss problem in 1-atmosphere gas mixing experiments: Theoretical and practical considerations. *Contributions to Mineralogy and Petrology* **78**, 298–304.

Grove, T. L. (1990). Cooling histories of lavas from Serocki volcano. *Proceedings of the Ocean Drilling Program, Scientific Results* **106/109**, 3–8.

Grove, T. L. & Beaty, D. W. (1980). Classification, experimental petrology and possible volcanic histories of the Apollo 11 high-K basalts. *Proceedings of the Eleventh Lunar and Planetary Science Conference*, 149–177.

Grove, T. L. & Bryan, W. B. (1983). Fractionation of pyroxene-phyric MORB at low pressure: An experimental study. *Contributions to Mineralogy and Petrology* **84**, 293–309.

Grove, T. L., Elkins-Tanton, L. T., Parman, S. W., Chatterjee, N., Müntener, O. & Gaetani, G. A. (2003). Fractional crystallization and mantle-melting controls on calc-alkaline differentiation trends. *Contributions to Mineralogy and Petrology* **145**, 515–533.

Grove, T. L., Gerlach, D. C. & Sando, T. W. (1982). Origin of calc-alkaline series lavas at Medicine Lake Volcano by fractionation, assimilation and mixing. *Contributions to Mineralogy and Petrology* **80**, 160–182.

Grove, T. L. & Juster, T. C. (1989). Experimental investigations of low-Ca pyroxene stability and olivine-pyroxene-liquid equilibria at 1-atm in natural basaltic and andesitic liquids. *Contributions to Mineralogy and Petrology* **103**, 287–305.

Grove, T. L. & Vaniman, D. T. (1978). Experimental petrology of very low Ti (VLT) basalts. *Mare Crisium; The View from Luna 24*, 445–471.

Hanson, B. & Jones, J. H. (1998). The systematics of Cr^{+3} and Cr^{+2} partitioning between olivine and liquid in the presence of spinel. *American Mineralogist* **83**, 669–684.

Herd, C. D. K., Schwandt, C. S., Jones, J. H. & Papike, J. J. (2002). An experimental and petrographic investigation of Elephant Moraine 79001 lithology A: Implications for its petrogenesis and the partitioning of chromium and vanadium in a martian basalt. *Meteoritics & Planetary Science* **37**, 987–1000.

Huebner, J. S., Lipin, B. R. & Wiggins, L. B. (1976). Partitioning of chromium between silicate crystals and melts. *Proceedings of the Seventh Lunar Science Conference*, 1195–1220.

Irving, A. J., Merrill, R. B. & Singleton, D. E. (1978). Experimental partitioning of rare earth elements and scandium among armalcolite, ilmenite, olivine and mare basalt liquid. *Proceedings of the Ninth Lunar and Planetary Science Conference*, 601–612.

Johnston, A. D. & Draper, D. S. (1992). Near-liquidus phase relations of an anhydrous high-magnesia basalt from the Aleutian Islands: Implications for arc magma genesis and ascent. *Journal of Volcanology and Geothermal Research* **52**, 27–41.

Jurewicz, A. J. G., Mittlefehldt, D. W. & Jones, J. H. (1993). Experimental partial melting of the Allende (CV) and Murchison (CM) chondrites and the origin of asteroidal basalts. *Geochimica et Cosmochimica Acta* **57**, 2123–2139.

Jurewicz, A. J. G., Mittlefehldt, D. W. & Jones, J. H. (1995). Experimental partial melting of the St Severin (LL) and Lost City (H) chondrites. *Geochimica et Cosmochimica Acta* **59**, 391–408.

Jurewicz, A. J. G. & Watson, E. B. (1988). Cations in olivine, Part 1: Calcium partitioning and calcium-magnesium distribution between olivines and coexisting melts, with petrologic applications. *Contributions to Mineralogy and Petrology* **99**, 176–185.

Juster, T. C., Grove, T. L. & Perfit, M. R. (1989). Experimental constraints on the generation of FeTi basalts, andesites, and rhyodacites at the Galapagos Spreading Center, 85°W and 95°W. *Journal of Geophysical Research* **94**, 9251–9274.

Kadik, A. A., Biggar, G. M., Lukanin, O. A. & Dmitriev, L. V. (1982). An experimental study of the crystallization of Atlantic tholeiites at a given oxygen fugacity. *Geochemistry International* **19**, 104–127.

Kennedy, A. K., Grove, T. L. & Johnson, R. W. (1990). Experimental and major element constraints on the evolution of lavas from Lihir Island, Papua New Guinea. *Contributions to Mineralogy and Petrology* **104**, 722–734.

Kilinc, A., Carmichael, I. S. E., Rivers, M. L. & Sack, R. O. (1983). The ferric-ferrous ratio of natural silicate liquids equilibrated in air. *Contributions to Mineralogy and Petrology* **83**, 136–140.

Kinzler, R. J. & Grove, T. L. (1985). Crystallization and differentiation of Archaean komatiite lavas from northeast Ontario: phase equilibrium and kinetic studies. *American Mineralogist* **70**, 40–51.

Kinzler, R. J., Grove, T. L. & Recca, S. I. (1990). An experimental study on the effect of temperature and melt composition on the partitioning of nickel between olivine and silicate melt. *Geochimica et Cosmochimica Acta* **54**, 1255–1265.

Kohut, E. J. & Nielsen, R. L. (2003). Low-pressure phase equilibria of anhydrous anorthite-bearing mafic magmas. *Geochemistry, Geophysics, Geosystems* **4**, 1057, doi:10.1029/2002GC000451.

Longhi, J. & Pan, V. (1988). A reconnaisance study of phase boundaries in low-alkali basaltic liquids. *Journal of Petrology* **29**, 115–147.

Longhi, J. & Pan, V. (1989). The parent magmas of the SNC meteorites. *Proceedings of the Nineteenth Lunar and Planetary Science Conference*, 451–464.

McKay, G. A. & Weill, D. F. (1977). KREEP petrogenesis revisited. *Proceedings of the Eighth Lunar Science Conference*, 2339–2355.

Merrill, R. B. & Williams, R. J. (1975). The system anorthite-forsterite-fayalite-silica to 2 kbar with lunar petrologic applications. *Proceedings of the Sixth Lunar Science Conference*, 959–971.

Murck, B. W. & Campbell, I. H. (1986). The effects of temperature, oxygen fugacity and melt composition on the behaviour of chromium in basic and ultrabasic melts. *Geochimica et Cosmochimica Acta* **50**, 1871–1887.

Nielsen, R. L., Davidson, P. M. & Grove, T. L. (1988). Pyroxene-melt equilibria: an updated model. *Contributions to Mineralogy and Petrology* **100**, 361–373.

Parman, S. W., Dann, J. C., Grove, T. L. & deWit, M. J. (1997). Emplacement conditions of komatiite magmas from the 3.49 Ga Komati Formation, Barberton Greenstone Belt, South Africa. *Earth and Planetary Science Letters* **150**, 303–323.

Rhodes, J. M., Lofgren, G. E. & Smith, D. P. (1979). One atmosphere melting experiments on ilmenite basalt 12008. *Proceedings of the Tenth Lunar and Planetary Science Conference*, 1025–1027.

Sack, R. O. & Carmichael, I. S. F. (1984). $Fe^2 \leftrightarrow Mg^2$ and $TiAl_2 \leftrightarrow MgSi_2$ exchange reactions between clinopyroxenes and silicate melts. *Contributions to Mineralogy and Petrology* **85**, 103–115.

Sack, R. O., Walker, D. & Carmichael, I. S. E. (1987). Experimental petrology of alkalic lavas: constraints on cotectics of multiple saturation in natural basic liquids. *Contributions to Mineralogy and Petrology* **96**, 1–23.

Sato, H. (1989). Mg-Fe partitioning between plagioclase and liquid in basalts of Hole 504B, ODP Leg 111; a study of melting at 1 atm. *Proceedings of the Ocean Drilling Program, Scientific Results* **111**, 17–26.

Shi, P. (1993). Low-pressure phase relationships in the system Na_2O-CaO-FeO-MgO-Al_2O_3-SiO_2 at 1100°C, with implications for the differentiation of basaltic magmas. *Journal of Petrology* **34**, 743–762.

Singletary, S. J. & Grove, T. L. (2003). Early petrologic processes on the ureilite parent body. *Meteoritics and Planetary Science* **38**, 95–108.

Singletary, S. J. & Grove, T. L. (2006). Experimental constraints on ureilite petrogenesis. *Geochimica et Cosmochimica Acta* **70**, 1291–1308.

Snyder, D., Carmichael, I. S. E. & Wiebe, R. A. (1993). Experimental study of liquid evolution in an Fe-rich, layered mafic intrusion: constraints of Fe-Ti oxide precipitation on the T-fO_2 and T-ρ paths of tholeiitic magmas. *Contributions to Mineralogy and Petrology* **113**, 73–86.

Snyder, D. A. & Carmichael, I. S. E. (1992). Olivine-liquid equilibria and the chemical activities of FeO, NiO, Fe_2O_3, and MgO in natural basic melts. *Geochimica et Cosmochimica Acta* **56**, 303–318.

Stolper, E. (1977). Experimental petrology of eucritic meteorites. *Geochimica et Cosmochimica Acta* **41**, 587–611.

Thy, P. (1991). High and low-pressure phase equilibria of a mildly alkalic lava from the 1965 Surtsey eruption: Experimental results. *Lithos* **26**, 223–243.

Thy, P. (1992). Low-pressure melting relations of a basalt from Hole 797C in the Yamato Basin of the Japan Sea. *Proceedings of the Ocean Drilling Program, Scientific Results* **127–128, Part 2**, 861–868.

Thy, P. (1995a). Experimental constraints on the evolution of transitional and mildly alkalic basalts: crystallization of spinel. *Lithos* **36**, 103–114.

Thy, P. (1995b). Low-pressure experimental constraints on the evolution of komatiites. *Journal of Petrology* **36**, 1529–1548.
Thy, P., Lesher, C. E. & Fram, M. S. (1998). Low pressure experimental constraints on the evolution of basaltic lavas from site 917, southeast Greenland continental margin. *Proceedings of the Ocean Drilling Program, Scientific Results* **152**, 359–372.
Thy, P., Lesher, C. E., Nielsen, T. F. D. & Brooks, C. K. (2006). Experimental constraints on the Skaergaard liquid line of descent. *Lithos* **92**, 154–180.
Thy, P., Lofgren, G. E. & Imsland, P. (1991). Melting relations and the evolution of the Jan Mayen magma system. *Journal of Petrology* **32**, 303–332.
Toplis, M. J. & Carroll, M. R. (1995). An experimental study of the influence of oxygen fugacity on Fe-Ti oxide stability, phase relations, and mineral-melt equilibria in ferro-basaltic systems. *Journal of Petrology* **36**, 1137–1170.
Toplis, M. J., Libourel, G. & Carroll, M. R. (1994). The role of phosphorus in crystallization processes of basalt: An experimental study. *Geochimica et Cosmochimica Acta* **58**, 797–810.
Tormey, D. R., Grove, T. L. & Bryan, W. B. (1987). Experimental petrology of normal MORB near the Kane Fracture Zone: 22°N–25°N, mid-Atlantic ridge. *Contributions to Mineralogy and Petrology* **96**, 121–139.
Walker, D. & Grove, T. (1993). Ureilite smelting. *Meteoritics* **28**, 629–636.
Walker, D., Kirkpatrick, R. J., Longhi, J. & Hays, J. F. (1976). Crystallization history of lunar picritic basalt sample 12002: Phase-equilibria and cooling-rate studies. *Geological Society of America Bulletin* **87**, 646–656.
Walker, D., Longhi, J., Stolper, E. M., Grove, T. L. & Hays, J. F. (1977). Slowly cooled microgabbros 15065 and 15555. *Proceedings of the Eighth Lunar Science Conference*, 964–966.
Walker, D., Shibata, T. & DeLong, S. E. (1979). Abyssal tholeiites from the Oceanographer Fracture Zone. *Contributions to Mineralogy and Petrology* **70**, 111–125.
Wang, Z. & Gaetani, G. A. (2008). Partitioning of Ni between olivine and siliceous eclogite partial melt: experimental constraints on the mantle source of Hawaiian basalts. *Contributions to Mineralogy and Petrology* **156**, 661–678.
Yang, H.-J., Kinzler, R. J. & Grove, T. L. (1996). Experiments and models of anhydrous, basaltic olivine-plagioclase-augite saturated melts from 0.001 to 10 kbar. *Contributions to Mineralogy and Petrology* **124**, 1–18.

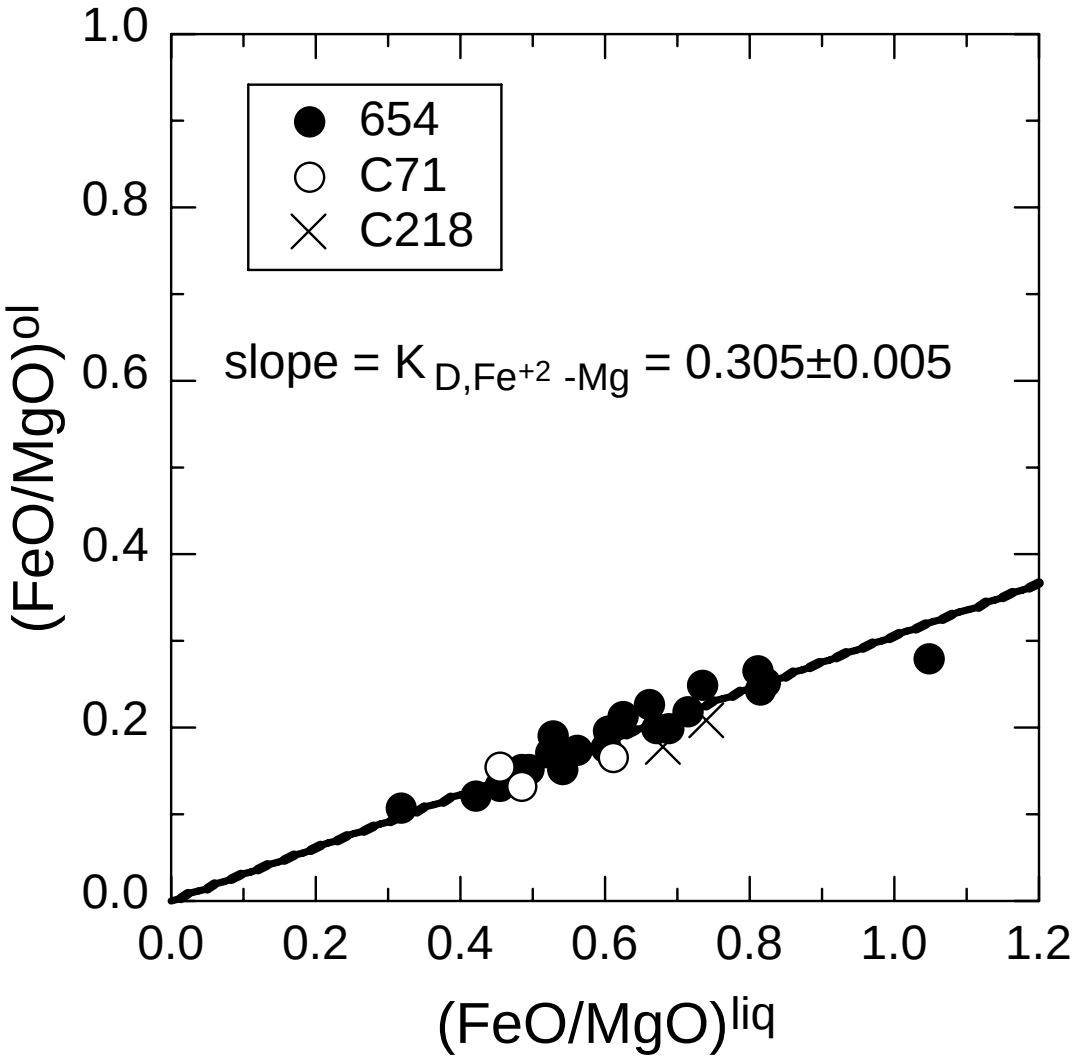

Fig. A1. Molar FeO/MgO in olivine (ol) vs. molar FeO/MgO in the coexisting liquid (liq) from the 27 experiments used by Roeder and Emslie (1970) to determine the value of the olivine-liquid Fe^{+2}-Mg exchange coefficient (K_D). Liquid FeO was determined by mass balance following the procedure described by Roeder and Emslie (1970): phases other than olivine and glass (spinel, clinopyroxene, and plagioclase) were ignored; the proportions of glass and olivine in each experiment were calculated using MgO contents of the glass, olivine, and bulk composition, respectively; FeO in the glass was calculated using the proportions of liquid and olivine and the measured FeO contents of the olivine and the bulk charge. The unweighted least-squares line is forced through the origin and yields a K_D of 0.305±0.005. The relative positions of the points are extremely similar to those seen in Fig. 4 of Roeder and Emslie (1970).

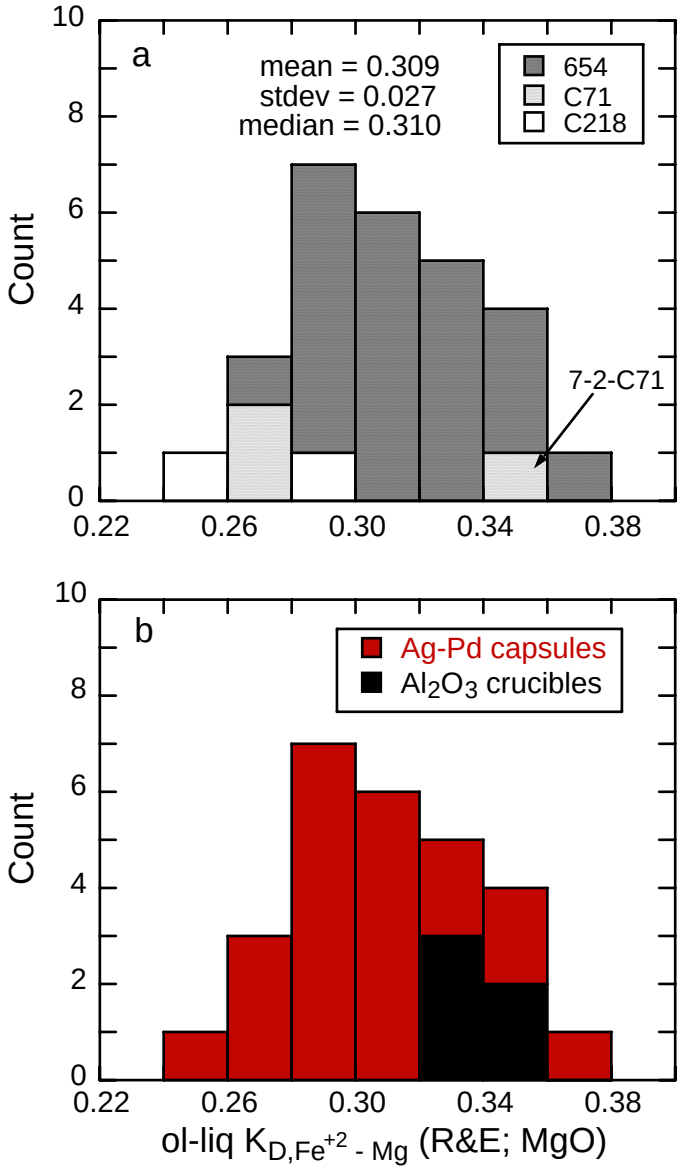

Fig. A2. (a) Histogram of individual ol-liq $K_{D,Fe^{+2}-Mg}$ values from the 27 experiments of Roeder and Emslie (1970); liquid FeO for each experiment calculated as described by Roeder and Emslie and in the caption to Fig. A1. The three different bulk compositions are denoted by dark (olivine basalt: 654), stippled (ankaramite: C71), and no shading (alkali olivine basalt: C218), respectively. The overall spread in K_D values is from 0.260 to 0.362. Although there is a tendency for experiments on the bulk compositions with lower silica contents (C71 and C218) to plot to the left of the diagram (to low K_Ds), one experiment on C71 produced a K_D of 0.343. (b) Histogram of individual ol-liq $K_{D,Fe^{+2}-Mg}$ values distinguished by capsule material: red = either $Ag_{55}Pd_{45}$ or $Ag_{60}Pd_{40}$ alloy capsules; black = Al_2O_3 crucibles. Note that the Al_2O_3 crucible experiments yield tightly clustered K_D values (0.344–0.327), while those from the Ag-Pd alloy runs range from 0.260–0.362.

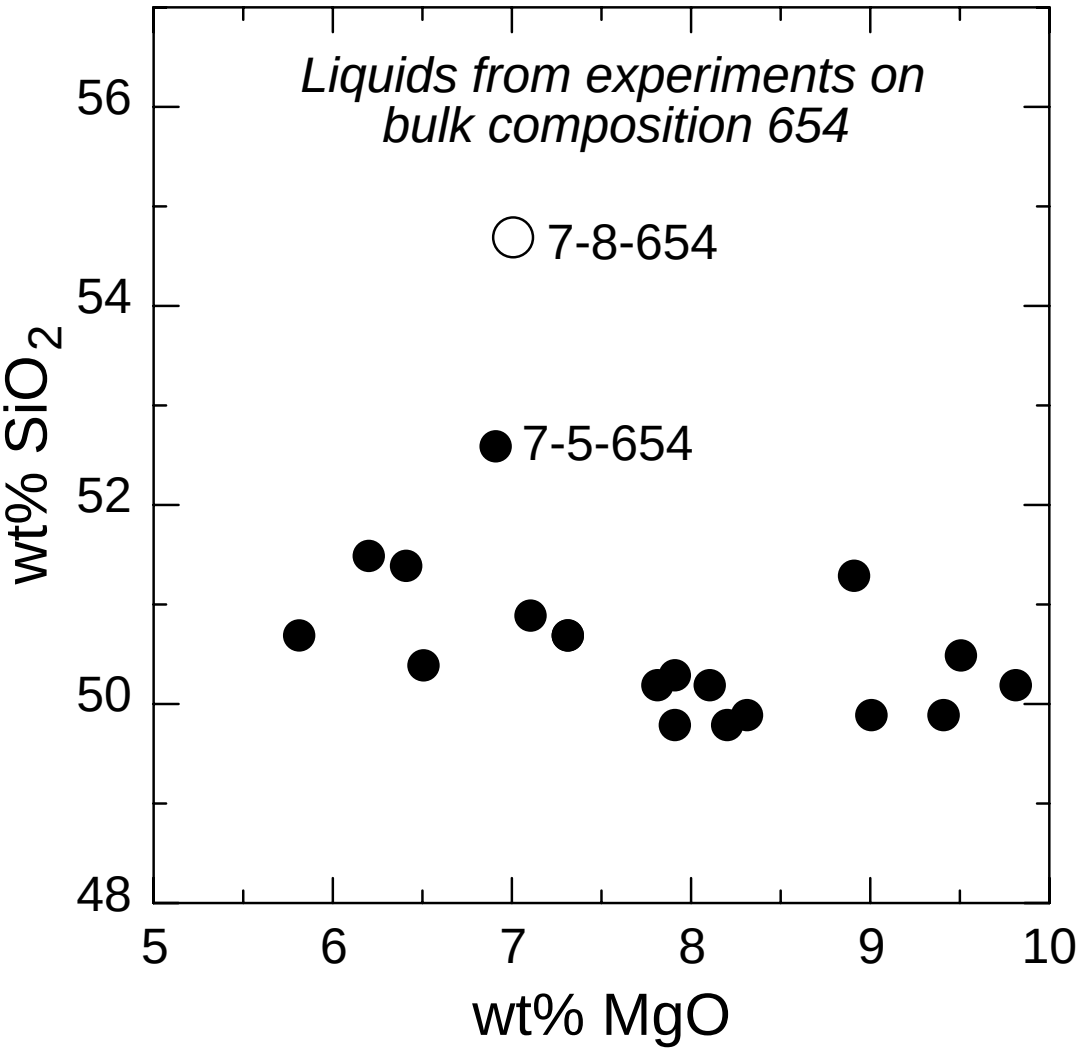

Fig. A3. SiO_2 vs. MgO (both in wt %) in the experimental glasses from the Kilauea olivine basalt (bulk composition 654) experiments showing the anomalous silica value in run 7-8-654 relative to the other glasses. Note that the SiO_2 content of the glass in 7-5-654 is also somewhat high relative to that seen in the remaining experiments.

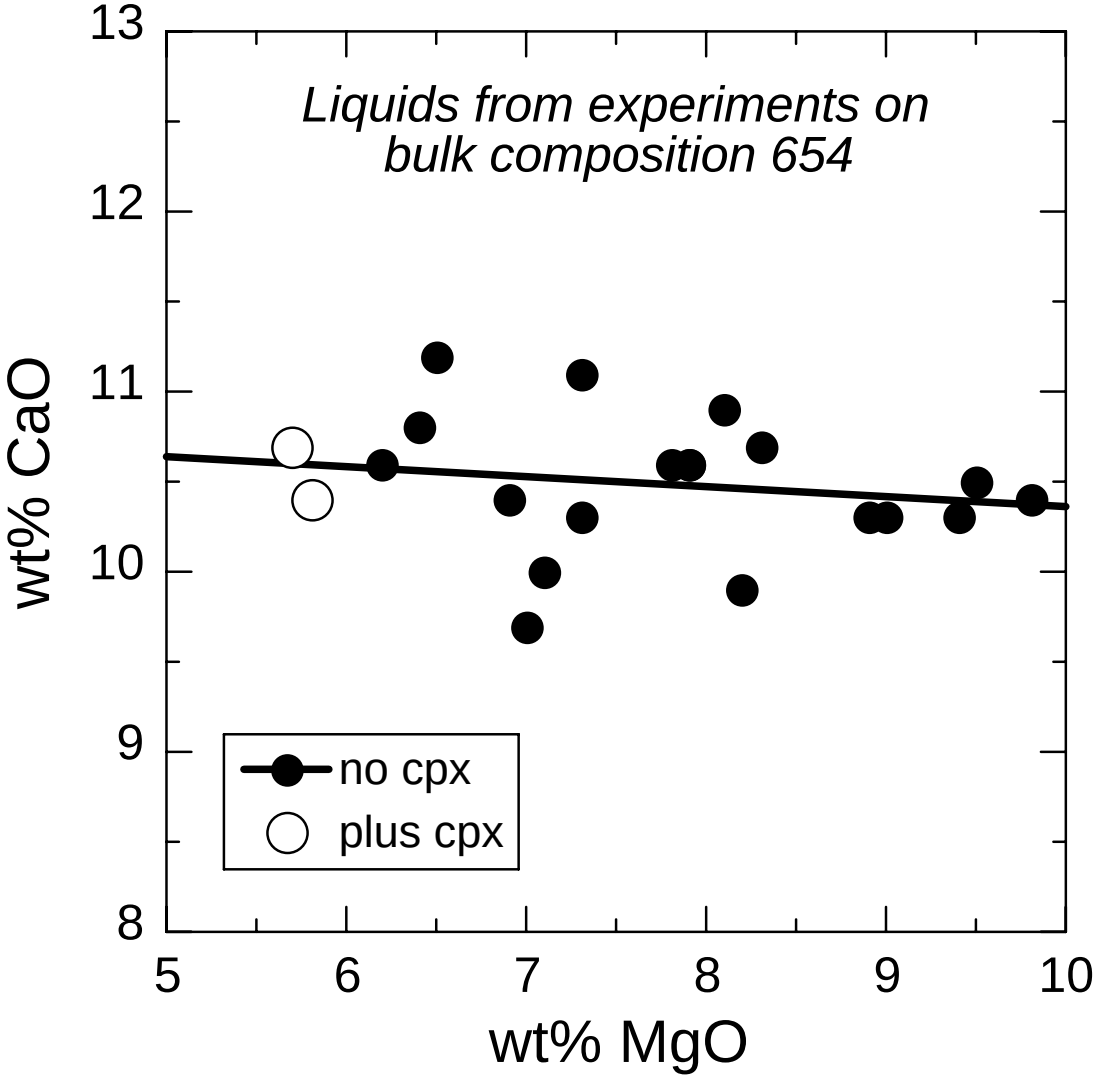

Fig. A4. CaO vs. MgO (both in wt %) in the experimental glasses from the olivine basalt (bulk composition 654) experiments showing that the two clinopyroxene (cpx)-bearing experiments (open circles) are consistent with the CaO-MgO trend defined by the clinopyroxene-free experiments (filled circles). The solid black line is an unweighted least-squares fit to the clinopyroxene-free glasses.

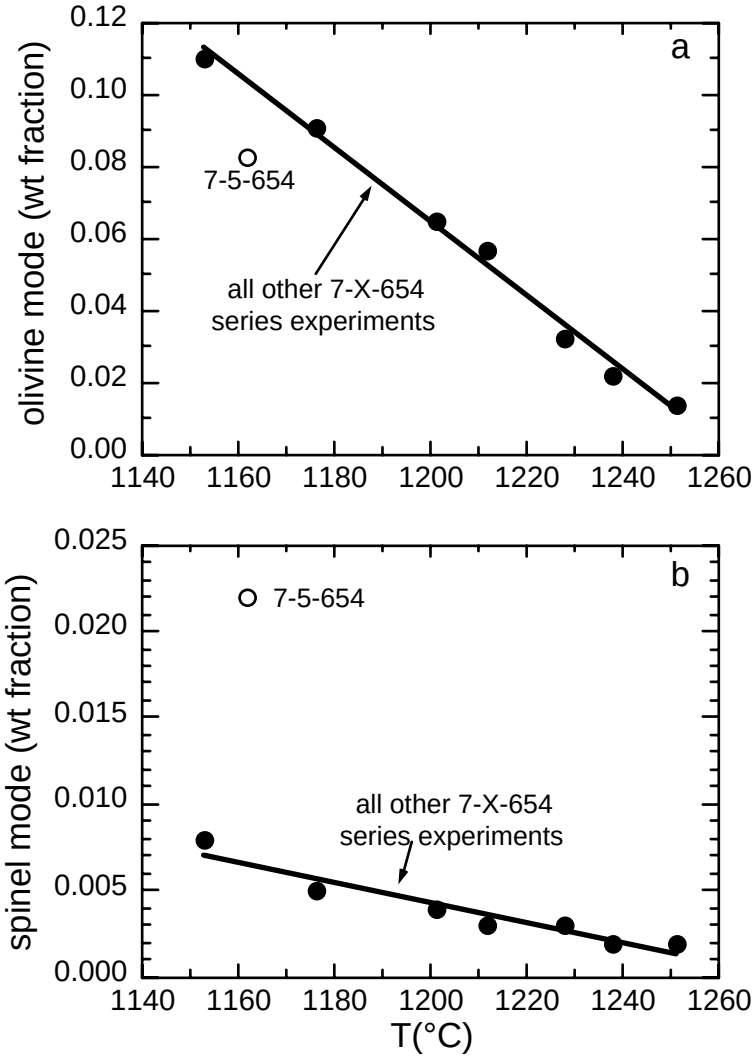

Fig. A5. Calculated olivine modes (a) and spinel modes (b) as a function of run temperature (°C). Only the 7-X-654 series of experiments are plotted (where X denotes the run number). Modes calculated using all oxides and all phases except clinopyroxene (this study). The filled circles define tight linear arrays that are negatively correlated with temperature, whereas run 7-5-654 plots substantially off the olivine and spinel trends. The calculated spinel mode for 7-5-654 is insensitive to the whether Cr-spinel or magnetite is used in the mass balance calculation.

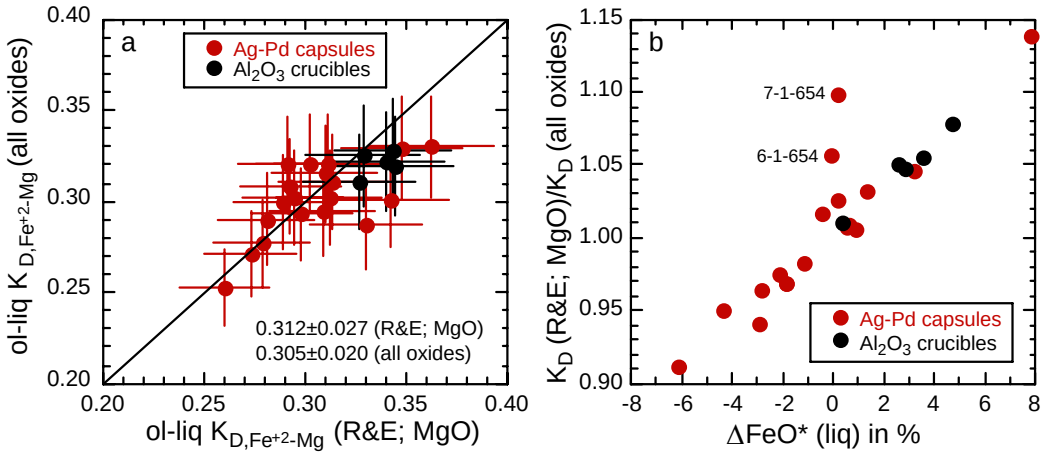

Fig. A6. (a) Olivine-liquid (ol-liq) $K_{D,Fe^{+2}-Mg}$(R&E; MgO) where liquid FeO is calculated using the approach of Roeder and Emslie (1970) vs. ol-liq $K_{D,Fe^{+2}-Mg}$ (all oxides) where liquid FeO is calculated using all oxides, a weighted mass balance approach, and with the compositions of all coexisting phases, except for clinopyroxene (this study). Symbol color denotes the experimental container material: either an Ag-Pd alloy or alumina. Error bars (1σ) for both sets of K_D values are calculated by propagating FeO and MgO uncertainties associated with liquid and olivine compositions (uncertainties in FeO liquid for the Roeder and Emslie K_Ds were assumed to be the same as those for FeO liquid in the complete mass balance calculation, see notes to Table A1 for more discussion). Unweighted mean and 1σ values for both sets of $K_{D,Fe^{+2}-Mg}$s are given in the lower right corner of the figure. Note that both mean values are based on 24 experiments (i.e., the three rejected experiments, 8-2-C218, 7-5-654 and 7-8-654 were not included in the $K_{D,Fe^{+2}-Mg}$ averages. (b) Ratio of K_Ds ($K_{D\ R\&E\ using\ MgO}/K_{D,\ using\ all\ oxides}$) vs. ΔFeO* liquid defined as the percentage difference between the calculated FeO + 0.89981×Fe_2O_3 value from the mass balance (mb) and the microprobe (probe) glass FeO* value for each experiment: $100\times[(FeO + 0.89981\times Fe_2O_3)_{mb} - FeO^*_{probe}]/FeO^*_{probe}$. Symbol color denotes the experimental container material (see legend).

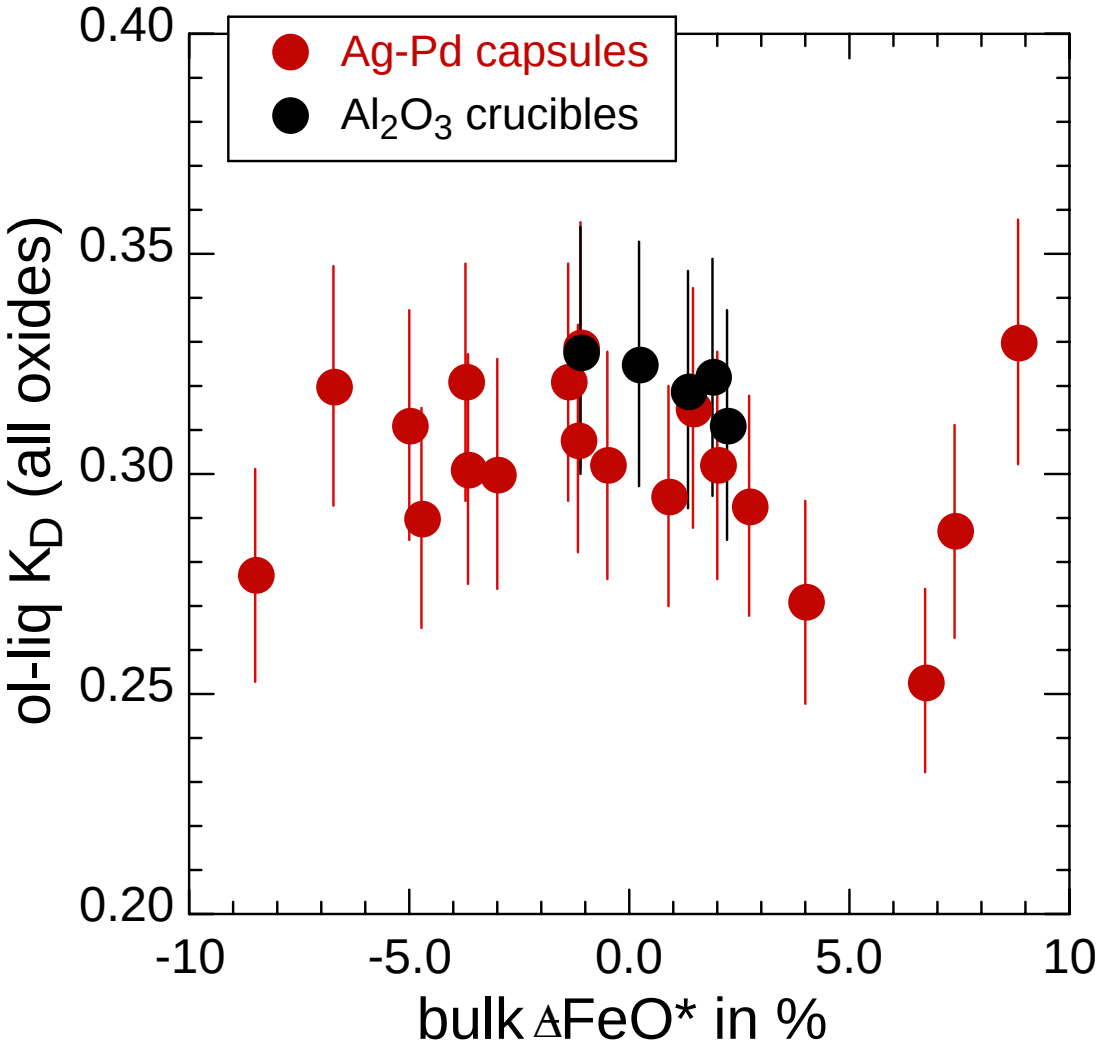

Fig. A7. Ol-liq $K_{D,Fe^{+2}-Mg}$s (liquid FeO for each experiment calculated using a weighted mass balance approach, all oxides, and all coexisting phases except clinopyroxene) vs. bulk ΔFeO* in percent. Bulk ΔFeO* is defined as the percent difference between the wet chemistry (wc) measurements on each experimental charge ($FeO + 0.89981 \times Fe_2O_3$) and FeO* measured by electron microprobe (probe) on each of the glassed starting materials: $100 \times [(FeO + 0.89981 \times Fe_2O_3)_{wc} - FeO^*_{probe}]/FeO^*_{probe}$. Symbol color denotes the run container: red for an Ag-Pd alloy or black for alumina. Error bars on $K_{D,Fe^{+2}-Mg}$ are 1σ and are based on FeO and MgO uncertainties in olivine and glass, respectively.

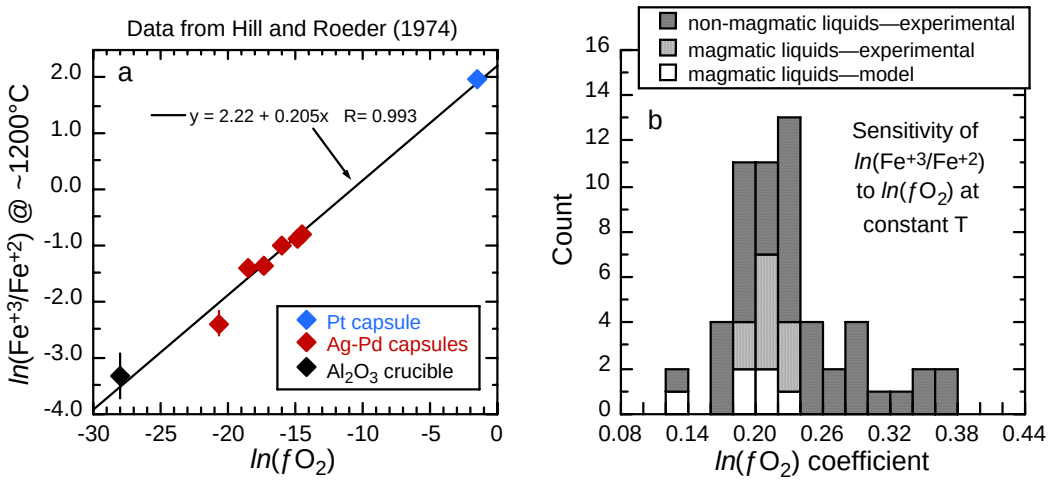

Fig. A8. (a) $ln(Fe^{+3}/Fe^{+2})$ molar vs. $ln fO_2$ for the ~1200°C superliquidus or near-liquidus experiments on bulk composition RHB (Hill and Roeder, 1974). FeO and Fe_2O_3 determined by wet chemistry (see Hill and Roeder, 1974 for a discussion of analytical methods). Temperature range for the eight experiments is 1195–1202°C; only the Pt capsule air experiment is below the liquidus. Error bars associated with $ln(Fe^{+3}/Fe^{+2})$ are one sigma and are based on the FeO and Fe_2O_3 uncertainties reported in Hill and Roeder (1974); for all but the two most reducing experiments, one sigma errors are smaller than the size of the symbols. (b) Histogram of $ln(fO_2)$ coefficients (the slope of the line in panel a) at constant temperature and liquid composition for a wide range of non-magmatic systems (e.g., iron oxide slags), magmatic liquids (e.g., natural silicate liquids), and model expressions designed for magmatic liquids (e.g., equations for estimating Fe^{+3}/Fe^{+2} as a function of temperature, fO_2, and liquid composition; the 654 bulk composition of Roeder and Emslie (1970) was used for calculating temperature dependences shown in the figure). Experimental data references: Larson and Chipman, 1953; Fudali, 1965; Shibata, 1967; Timucin and Morris, 1970; Hill and Roeder, 1974; O'Horo and Levy, 1978; Schreiber *et al*., 1980; Bowker *et al*., 1981; Mysen and Virgo, 1983; Virgo *et al*., 1983; Mysen *et al*., 1984; Schreiber *et al*., 1986; Dingwell and Virgo, 1987; Kress and Carmichael, 1988, 1989; Iwase *et al*., 1998; references for Fe^{3+}/Fe^{2+} models: Sack *et al*., 1980; Kilinc *et al*., 1983; Kress and Carmichael, 1988; Kress and Carmichael, 1991; Nikolaev *et al*., 1996; Jayasuriya *et al*., 2004.

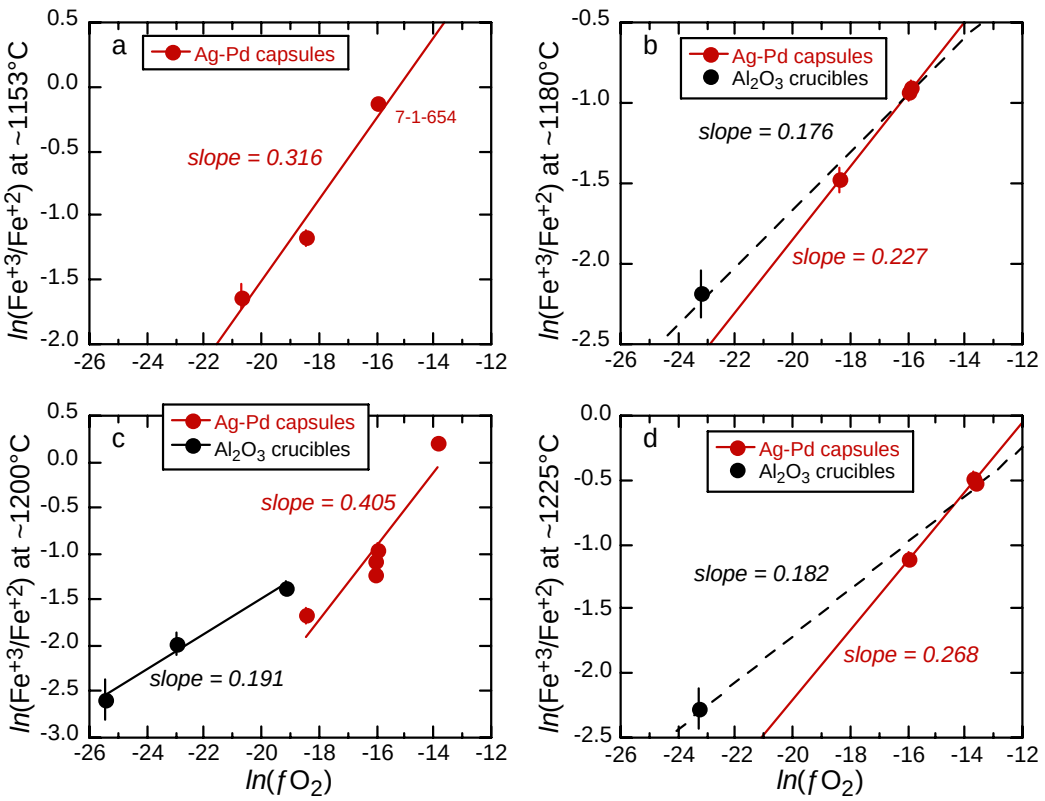

Fig. A9. Calculated $ln(Fe^{+3}/Fe^{+2})$ in glass vs. $ln(fO_2)$ for the experiments of Roeder and Emslie (1970) on the 654 bulk composition; liquid Fe_2O_3 and FeO from mass balance calculations using all oxides and phases (except clinopyroxene). Experiments from 1152–1153°C are plotted in (a), from 1175–1180°C in (b), from 1195–1212°C in (c), and from 1214–1228°C in (d). Regression lines and accompanying slopes are unweighted fits to the data: red solid lines are fits to the Ag-Pd capsule experiments plotted in each panel; solid black lines are fits to the Al_2O_3 crucible experiments; and black dashed lines are fits to all the points in a given panel. Error bars (often smaller than the size of the symbols) are one sigma and are based on estimates of the uncertainties associated with the calculated FeO and Fe_2O_3 in the glass (see text for further discussion).

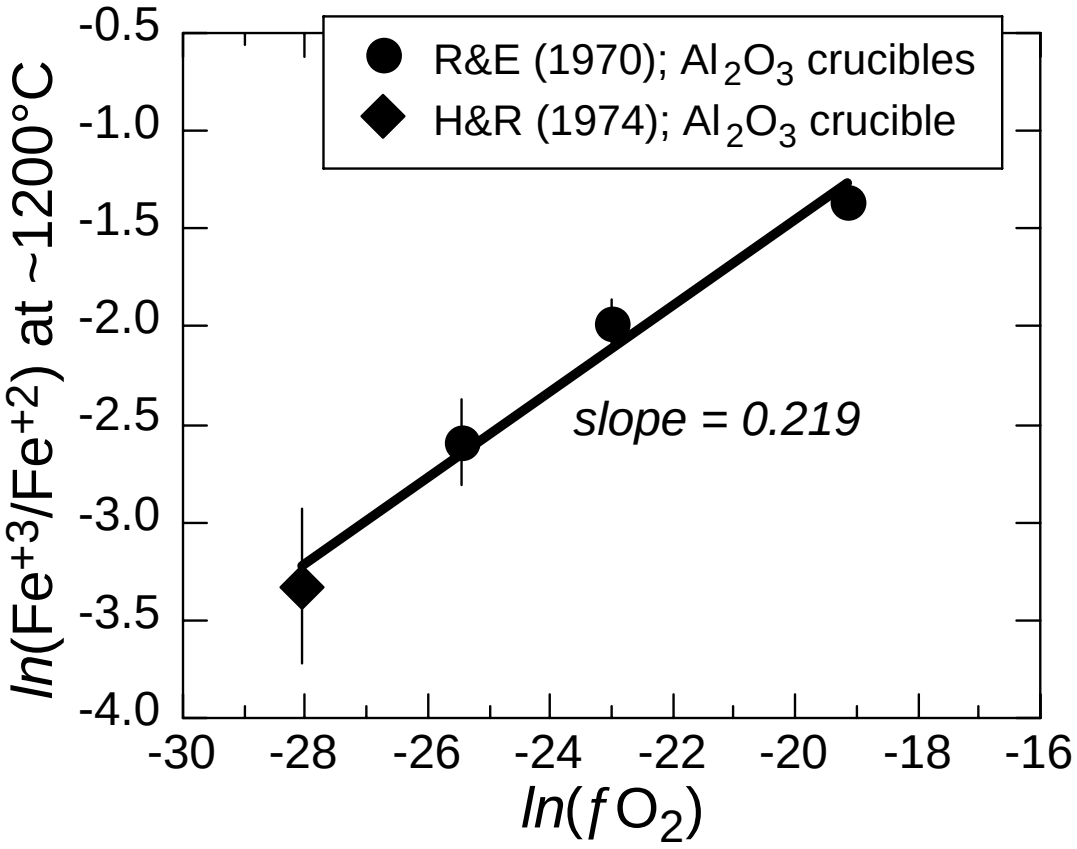

Fig. A10. $ln(Fe^{+3}/Fe^{+2})$ vs. $ln(fO_2)$ for the ~1200°C alumina crucible experiments on bulk composition 654 (Roeder and Emslie, 1970) and RHB (Hill and Roeder, 1974). Slope is from an unweighted fit to the data; error bars are one sigma and are calculated as described in the caption to Fig. A9.

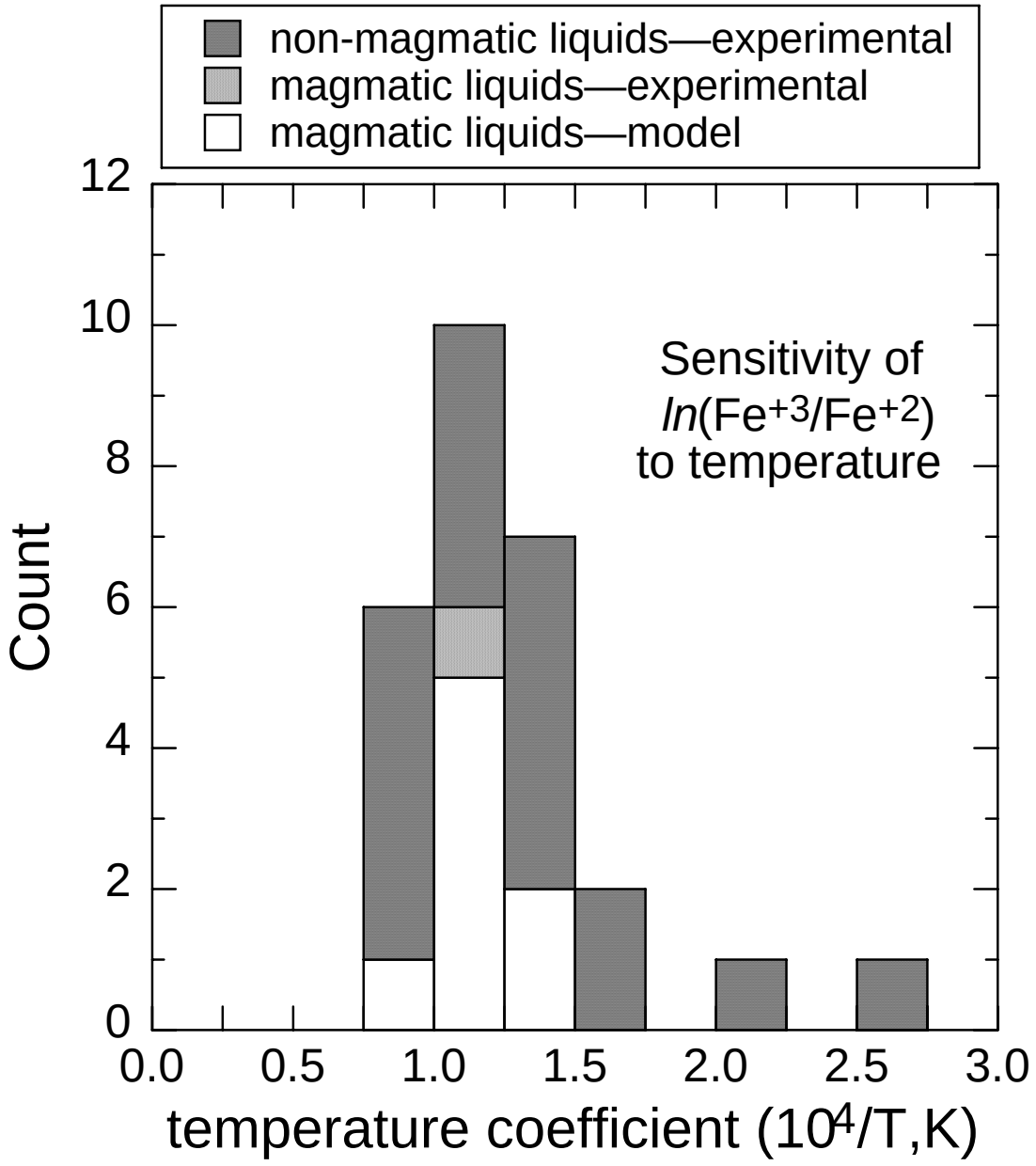

Fig. A11. Histogram of temperature coefficients (10^4/T, K) for $ln(Fe^{+3}/Fe^{+2})$ in non-magmatic and magmatic liquids and from model expressions (e.g., equations for estimating Fe^{+3}/Fe^{+2} as a function of temperature, fO_2, and liquid composition). Data sources: Kennedy (1948), Johnston (1964), Sack *et al*. (1980), Kilinc *et al*. (1983), Mysen and Virgo (1983), Mysen *et al*. (1985ab), Kress and Carmichael (1988, 1991), Borisov and Shapkin (1989), Ghiorso and Kress (2004), Lange and Carmichael (1989), Ohashi *et al*. (2000), and Jayasuriya *et al*. (2004).

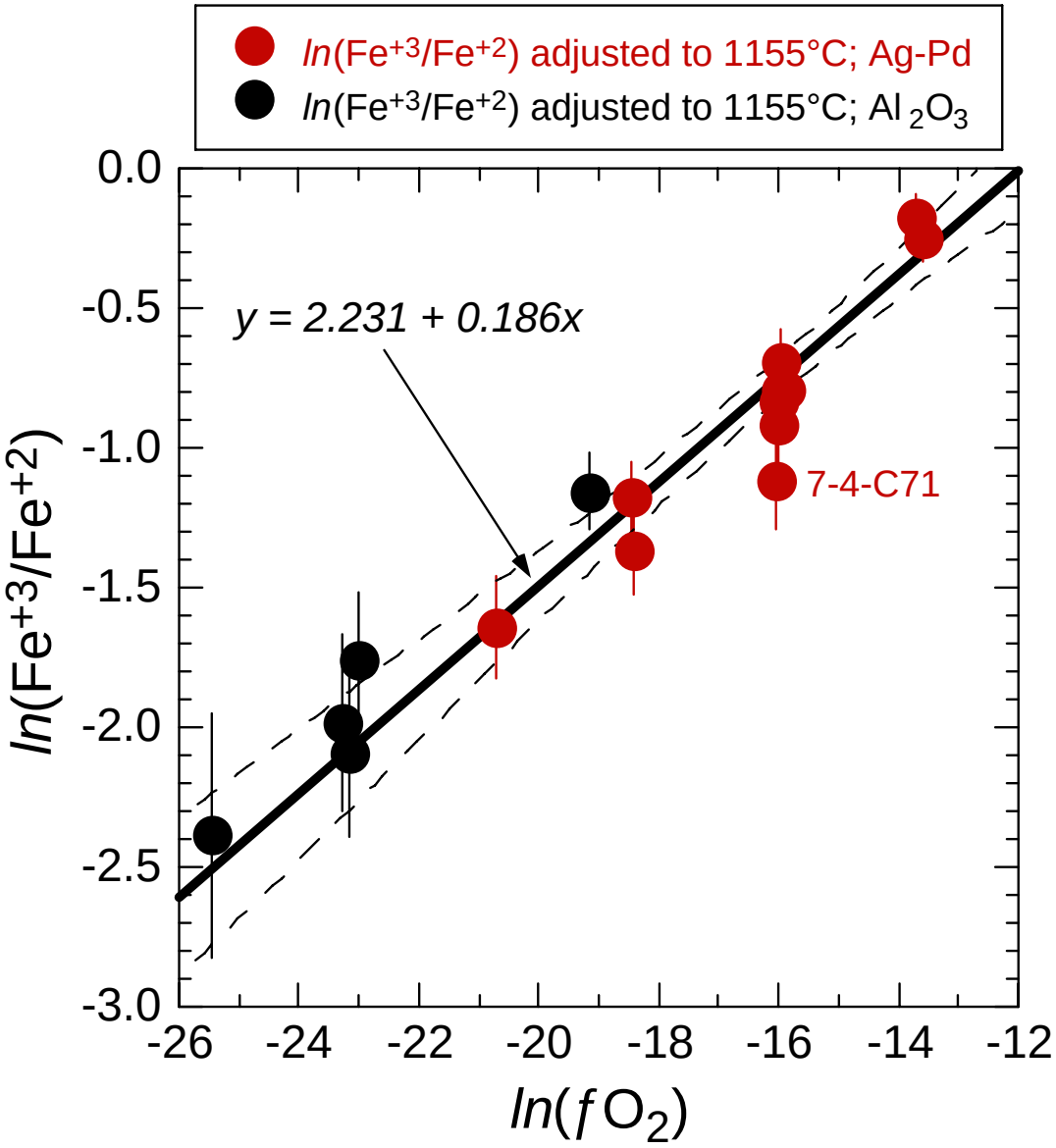

Fig. A12. $ln(Fe^{+3}/Fe^{+2})$ corrected to a reference temperature of 1155°C vs. $ln(fO_2)$ for the five alumina and 12 Ag-Pd experiments that have provisionally passed all of the previously described tests that are described in the text. The solid line is a weighted fit to the data and the dashed curves represent the 95% confidence interval for the regression. Error bars associated with each point are 2σ and are calculated as described in the caption to Fig. A9.

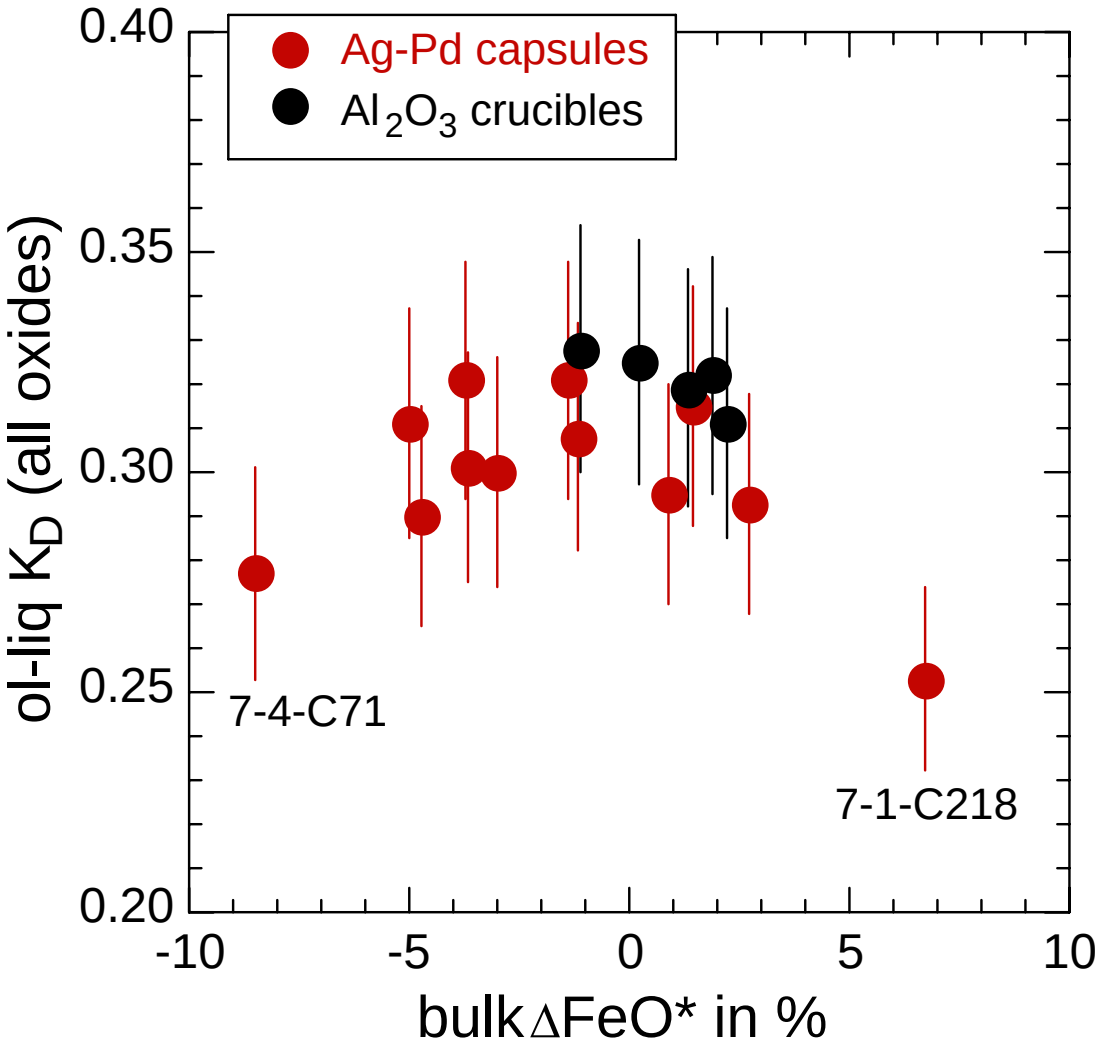

Fig. A13. $K_{D,Fe^{+2}-Mg}$s (liquid FeO for each experiment calculated using a weighted mass balance approach, all oxides, and all coexisting phases except clinopyroxene) vs. bulk ΔFeO* in percent (defined in the caption to Fig. A7). Error bars are 1σ and are calculated as described in the caption to Fig. A6. Only the experiments plotted in Fig. A12 are shown here. Compare to Fig. A7.

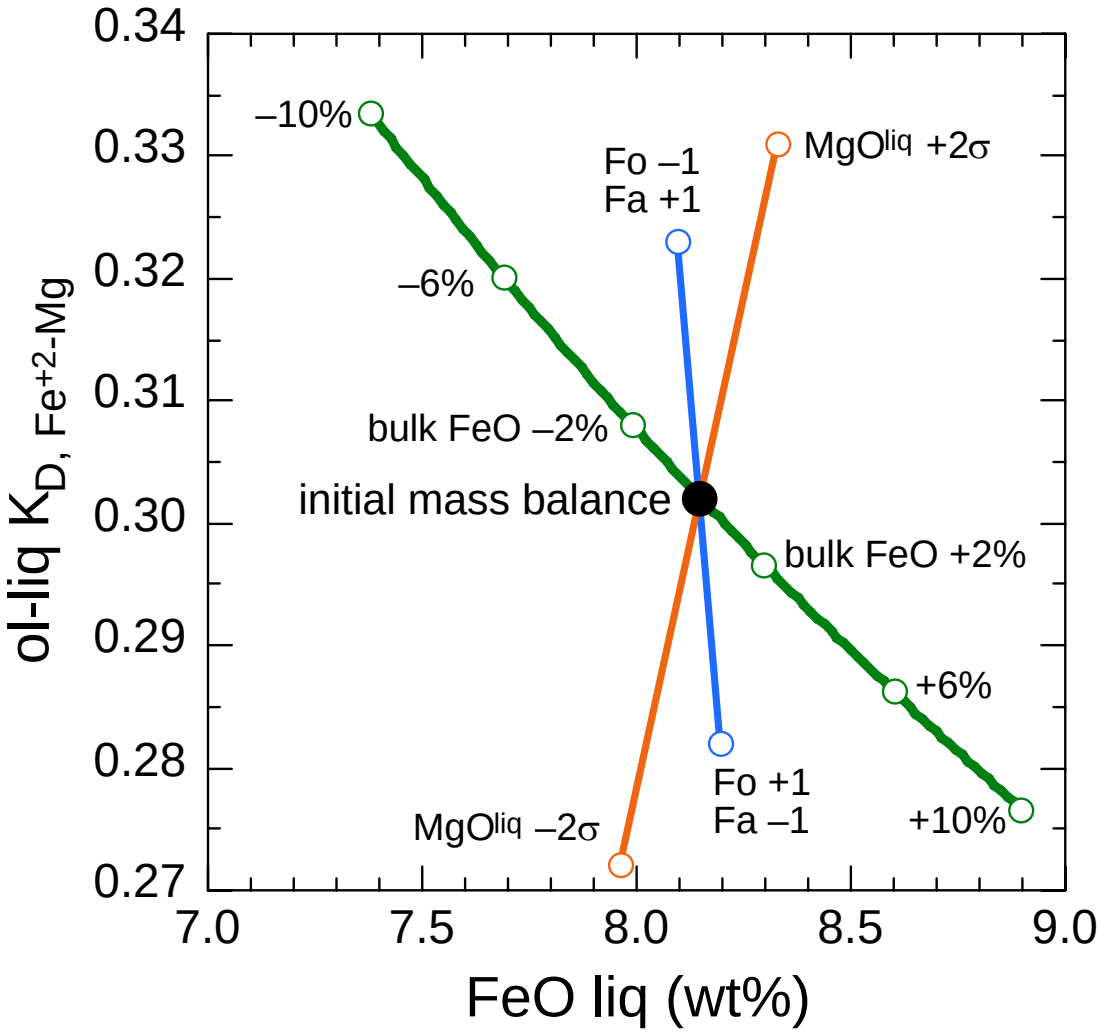

Fig. A14. The sensitivity of $K_{D,Fe^{+2}-Mg}$ to changes in bulk FeO, liquid MgO, and Fo and Fa contents of the equilibrium olivine. The filled black circle is the result of the mass balance calculation for run 7-3-654 (Table A1). The green curve denotes the effect on $K_{D,Fe^{+2}-Mg}$ and liquid FeO of increasing or decreasing the bulk FeO by the specified amount and rerunning the mass balance. Changing the olivine composition from $Fo_{79}Fa_{20}$ to either $Fo_{78}Fa_{21}$ or $Fo_{80}Fa_{19}$ (weight units) and rerunning the mass balance results in the open blue circles. The effect of changing the liquid MgO content by ±2σ is denoted by the open orange circles (uncertainties for bulk FeO and liquid MgO are listed in the notes to Table A1.

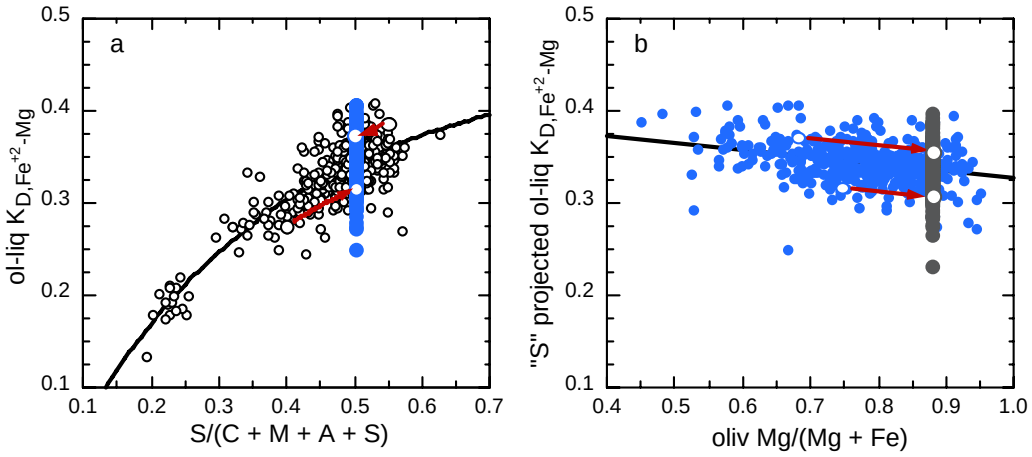

Fig. A15. (a) S/(C + M + A + S) vs. ol-liq $K_{D,Fe^{+2}-Mg}$ for the 1-atm QFM±0.25 experiments compiled from the literature as part of this study. Small open black circles are data from the literature; S/(C + M + A + S) calculated as described in the Supplement; $K_{D,Fe^{+2}-Mg}$ calculated using FeO in each of the glass compositions as predicted by Jayasuriya *et al.*, 2004 at the temperature and fO_2 of that experiment. The curved black line is an unweighted least-squares fit to this data using the expression: $K_{D,Fe^{+2}\text{-}Mg} = a + b \times \exp(c \times \text{“S”})$ where “S” is equal to S/(C + M + A + S), the values of the coefficients a, b, and c are given in the Supplement. The two larger open black circles are representative points that illustrate the effect of being moved parallel to the black line (path denoted by the two red lines with arrows) to an “S” value of 0.5; their projected positions are given by the two open blue circles. The smaller filled blue circles represent the projected positions of all the other open black circles. (b) “S” projected ol-liq $K_{D,Fe^{+2}-Mg}$ ($[K_{D,Fe^{+2}\text{-}Mg}]_{0.5}$) vs. coexisting olivine Mg/(Mg+Fe), atomic, values. The filled and open blue circles are the same as those in Fig. A15a. The black line is an unweighted least-squares fit using the equation: $[K_{D,Fe^{+2}\text{-}Mg}]_{0.5} = d + e \times [Mg/(Mg+Fe)]^{ol}$ (values of the coefficients are given in the Supplemental text). Red lines show the movement of two representative points (the same two points as in panel a) parallel to the black line to an olivine composition of Fo_{88}. This represents the second projection. The filled gray circles define the now twice-projected ol-liq K_D values. It is these twice-projected values that are plotted in histogram form in Fig. 4 in the main article.

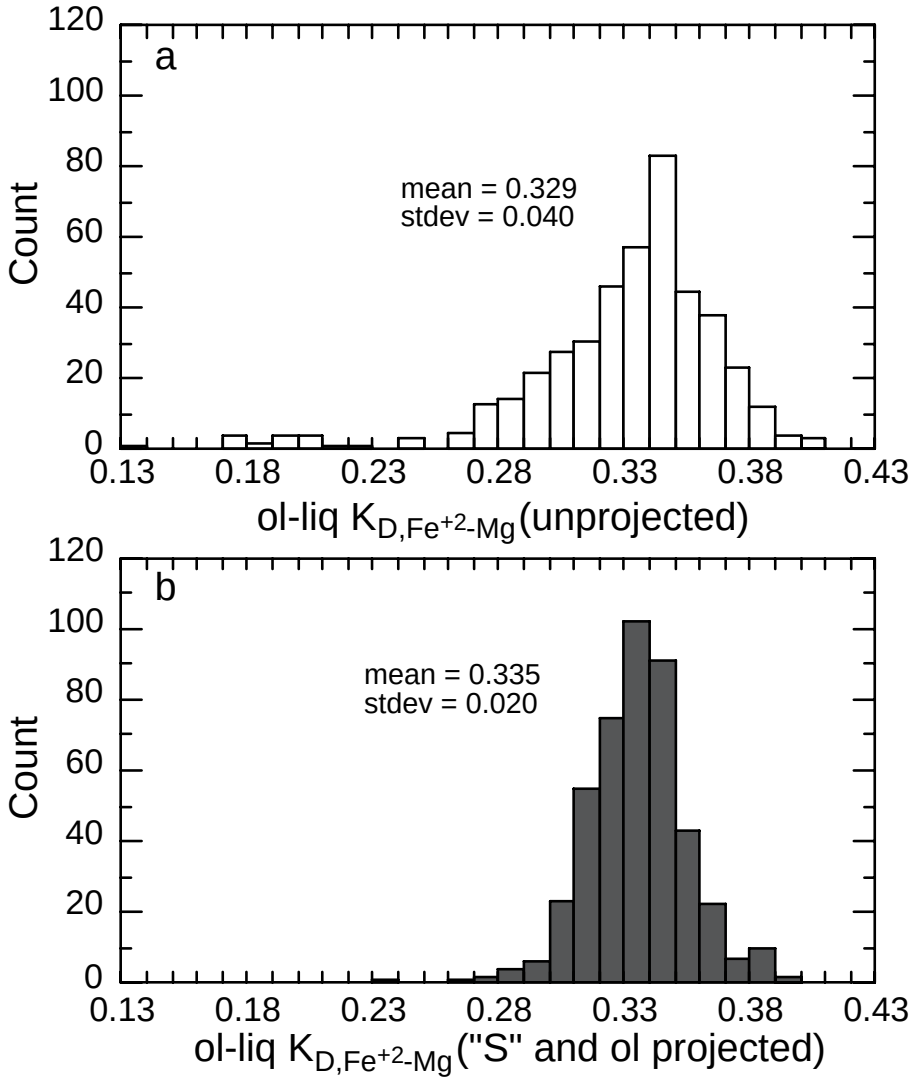

Fig. A16. A comparison of unprojected ol-liq $K_{D,Fe^{+2}-Mg}$s (a) and "S" and olivine Mg# projected values (b); both sets of $K_{D,Fe^{+2}-Mg}$s calculated using experiments from the literature at QFM±0.25 and eqn 12 of Jayasuriya *et al*. (2004) to estimate the FeO content of the experimental glasses. The mean and standard deviation (stdev) for each set of $K_{D,Fe^{+2}-Mg}$s is listed in each panel.

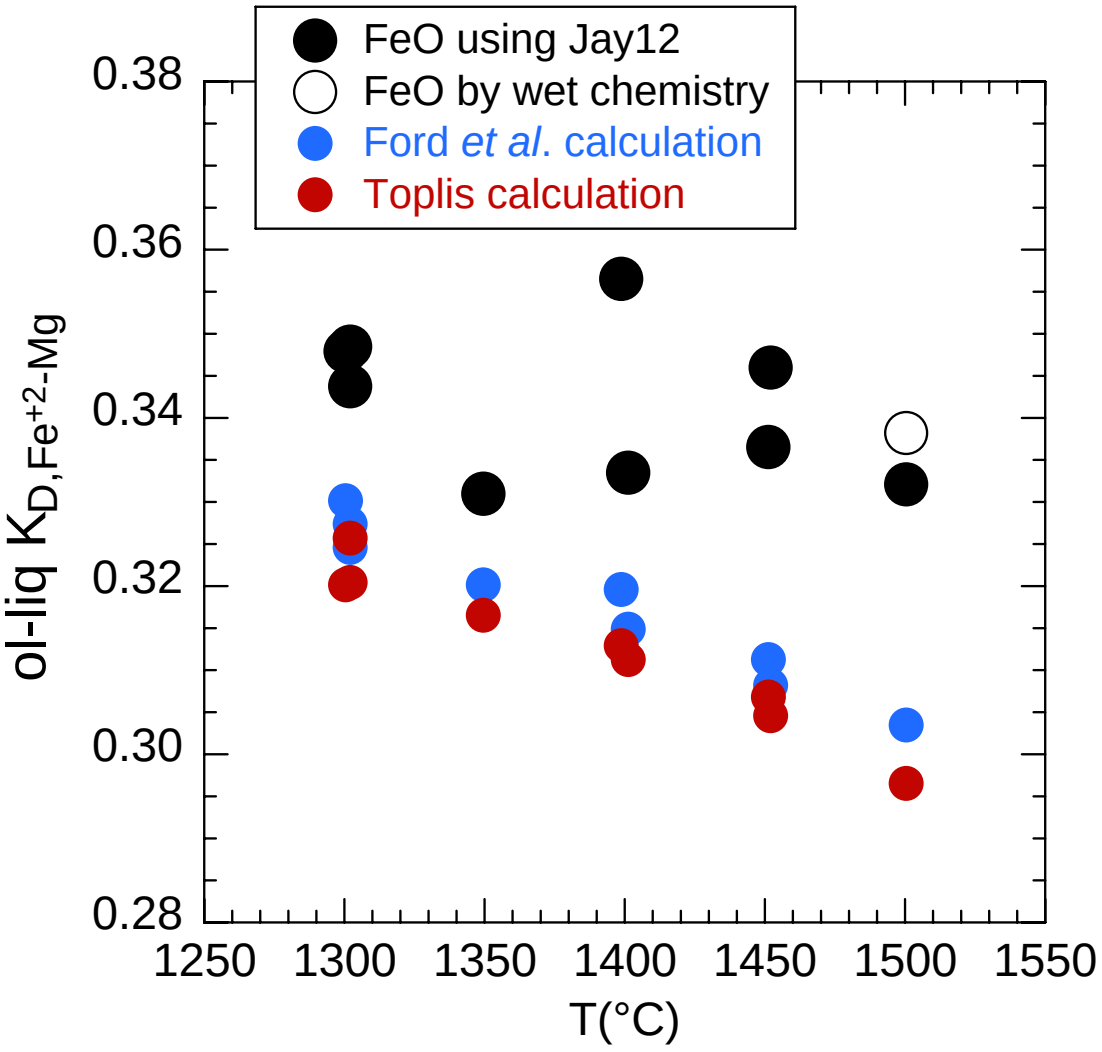

Fig. A17. Ol-liq $K_{D,Fe^{+2}-Mg}$s as a function of temperature comparing $K_{D,Fe^{+2}\text{-}Mg}$s calculated using olivine and liquid compositions from the experiments from this study to those calculated using the parameterizations of Ford *et al*. (1983) and Toplis (2005). Filled black circles are calculated using liquid FeO contents as estimated by eqn 12 of Jayasuriya *et al*. (2004), liquid MgO contents, and olivine compositions; open circle indicates the $K_{D,Fe^{+2}\text{-}Mg}$ calculated using the wet chemistry FeO liquid determination. Blue and red circles are $K_{D,Fe^{+2}\text{-}Mg}$s calculated using the temperatures, fO_2s, and liquid compositions of the experiments and the parameterizations of Ford *et al*. (1983) and Toplis (2005), respectively.

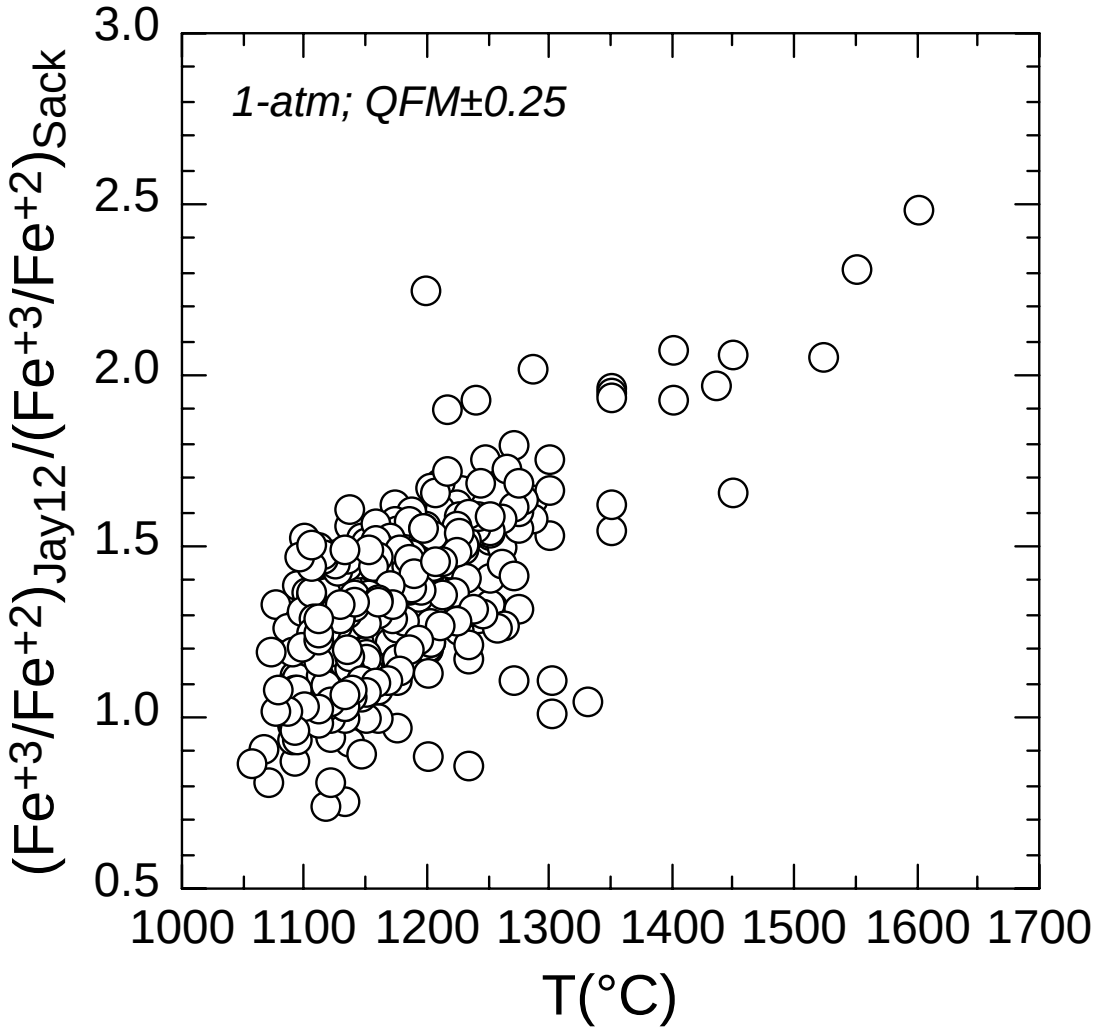

Fig. A18. $(Fe^{+3}/Fe^{+2})_{Jay12}/(Fe^{+3}/Fe^{+2})_{Sack}$ (molar) vs. temperature (°C) of the experimental glasses from the 1-atm QFM±0.25 data set compiled as part of this study. "Jay12" and "Sack" in the y-axis label refer to Jayasuriya *et al*. (2004) eqn 12 and Sack *et al*. (1980), respectively.

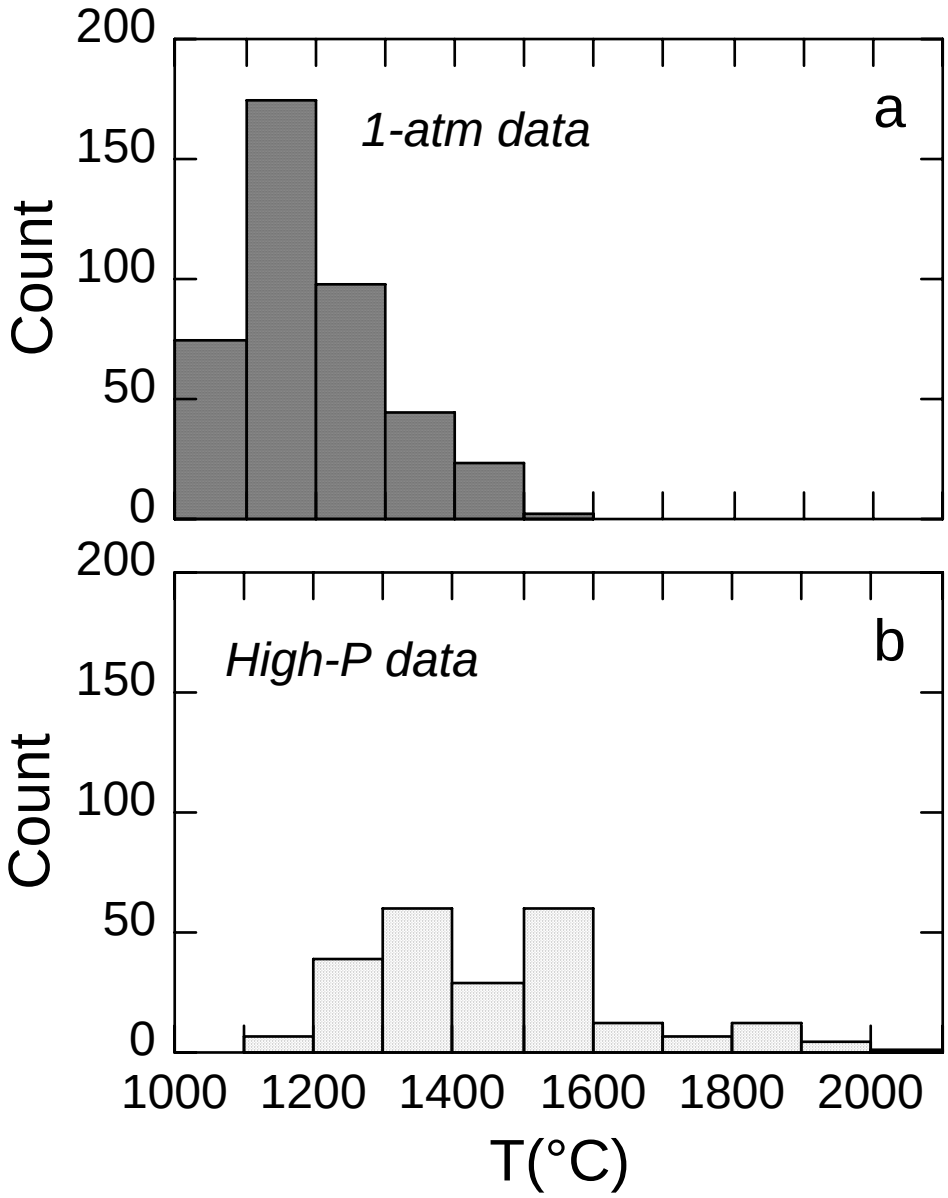

Fig. A19. Distribution of run temperatures from 1-atm experiments (a) and high-pressure experiments (b) included in the calibration data set of the Toplis (2005) olivine-liquid Fe^{+2}-Mg exchange model. Literature references are from the captions to Fig. 1, 8, 9, and 10 of Toplis, and we assumed that all olivine-liquid-bearing experiments from these sources were used. The pressure range in panel (b) is from 5 to 144 kbar and pressure and temperature show a strong positive correlation.

Table A1. Results of the mass balance calculations using the experimental data of Roeder and Emslie (1970)

Run #	liq	ol	sp	plag	liq FeO	liq Fe_2O_3	χ^2	SSR	bulkΔFeO*	K_D^{all}	K_D^{mg}	ΔQFM
7-1-654	0.882	0.110	***0.008***		5.979	5.878	1.12	0.62	8.85	0.330(28)	0.362(31)	2.06
7-2-654	0.904	0.091	0.005		7.903	3.464	2.71	0.10	2.73	0.293(25)	0.298(25)	1.75
7-3-654	0.931	0.065	0.004		8.146	3.515	0.50	0.17	2.03	0.302(26)	0.312(26)	1.46
7-5-654	0.895	0.083	***0.022***		7.406	3.611	1.43	0.94	7.40	0.287(24)	0.330(28)	1.92
7-6-654	0.966	0.032	0.003		8.295	3.042	1.18	0.33	–4.70	0.290(25)	0.281(24)	1.17
7-9-654	0.940	0.057	0.003		8.268	3.148	1.73	0.09	–0.50	0.302(26)	0.294(25)	1.30
7-10-654	0.976	0.022	0.002		8.262	2.894	0.17	0.02	–5.02	0.311(26)	0.314(27)	1.03
7-11-654	0.984	0.014	0.002		8.351	3.084	0.46	0.10	–3.74	0.321(27)	0.311(26)	0.89
6-1-654	0.952	0.043	***0.005***		4.945	6.695	0.19	0.07	–1.12	0.329(28)	0.348(30)	2.45
6-2-654	0.974	0.020	0.006		6.804	4.678	0.82	0.20	–3.01	0.300(26)	0.289(25)	2.18
6-3-654	0.967	0.026	0.007		6.942	4.619	1.69	0.29	–1.16	0.308(26)	0.293(25)	2.34
8-1-654	0.815	0.122	0.004	0.058	8.456	2.927	2.09	1.12	–1.38	0.321(27)	0.302(26)	0.96
8-2-654	0.912	0.085	0.003		9.115	2.320	0.36	0.30	1.42	0.315(27)	0.310(26)	0.68
8-3-654	0.942	0.056	0.002		9.027	1.888	3.76	0.86	–6.72	0.320(27)	0.292(25)	0.39
8-4-654	0.934	0.063	0.003		8.817	2.507	0.86	0.22	2.20	0.311(26)	0.327(28)	0.07
9-1-654	0.841	0.143		0.015	8.695	1.896	3.62	1.10	0.89	0.295(25)	0.309(26)	–0.01
10-3-654	0.951	0.049			9.562	1.096	1.65	1.25	–1.10	0.328(28)	0.344(29)	–1.94
10-4-654	0.921	0.079			9.270	1.423	3.28	1.88	1.31	0.319(27)	0.344(29)	–1.64
10-5-654	0.892	0.106	0.002		9.334	1.166	0.44	0.47	0.21	0.325(28)	0.328(28)	–1.35
11-2-654	0.911	0.089			9.789	0.819	3.03	1.86	1.87	0.322(27)	0.340(29)	–2.65
7-1-C71	0.918	0.079	0.003		8.970	2.903	1.35	0.62	4.01	0.271(23)	0.273(23)	1.30
7-2-C71	0.941	0.056	0.003		8.189	2.546	8.36	2.70	–3.68	0.301(26)	0.343(29)	1.03
7-4-C71	0.962	0.036	0.002		8.745	1.983	0.99	1.26	–8.51	0.277(24)	0.279(24)	0.69
7-1-C218	0.955	0.040	***0.005***	0.000	8.474	3.811	0.74	0.92	6.73	0.253(21)	0.260(22)	1.75

Notes: Bold and italicized run numbers indicate experiments conducted in alumina crucibles; all other experiments were conducted in Ag-Pd alloy capsules. Phase abbreviations: liq = liquid, ol = olivine, sp = Cr-spinel or magnetite, plag = plagioclase; values under these heading are phase proportions in weight fractions; values in bold and italics under the sp-heading indicate magnetite. In run 7-1-C218, the mass balance calculation returned a plagioclase mode of zero; the qualitative plagioclase mode in Roeder and Emslie's unpublished data table (REUPDT) is "trace". Liquid FeO and liquid Fe_2O_3 are the wt % concentrations of these oxides in the liquid calculated by mass balance. SSR = sum of squared residuals from the mass balance. BulkΔFeO* is the difference (in %) between the bulk FeO* content determined by microprobe (probe) on each of the glassed starting materials and the wet chemistry (wc) bulk FeO and Fe_2O_3 measurements on each of the experimental charges: $100 \times [(FeO + 0.89981 \times Fe_2O_3)_{wc} - FeO^*_{probe}]/FeO^*_{probe}$. K_D^{all} is the olivine-liquid exchange coefficient calculated using liquid FeO content based on a mass balance using all oxides and phases with the exception that clinopyroxene in runs 7-1-654 and 9-1-654 were assumed to be negligible; K_D^{mg} is the exchange coefficient with liquid FeO determined following the procedure of Roeder and Emslie (1970). Values in parentheses are 1σ uncertainties calculated by propagating the 1σ errors associated with FeO and MgO in liquid and olivine, respectively; uncertainties on the phase compositions are described below. ΔQFM is the $log fO_2$ of the experiment relative to the QFM buffer (O'Neill, 1987). Bulk compositions for the three starting materials are from Table 1 of Roeder and Emslie (1970) with the exception that the bulk FeO* value in each mass balance calculation was replaced by the wet chemical measurements of bulk FeO and Fe_2O_3 for each experiment; wet chemical data are taken from REUPDT. Cr contents for the three bulk compositions (not reported in Table 1 of Roeder and Emslie, 1970) were estimated using Cr and MgO contents for lavas from Kilauea (1084 points) and Hualalai (77 points) from the GeoRoc database (http://georoc.mpch-mainz.gwdg.de/georoc/). The equation: Cr (ppm) = a + b $\times log$(MgO, wt%), yielded fits with correlation coefficients (R) of 0.95 (Kilauea) and 0.90 (Hualalai), respectively and Cr_2O_3 contents in wt % of 0.0879 (Kilauea, 654), 0.0604 (Hualalai, C218), and 0.1009 (Hualalai, C71) for the MgO contents of the three bulk compositions; a and b values for the two sets of data are: –1375.17, 1959.79 (Kilauea) and –1705.77, 2318.70 (Haulalai). Olivine compositions are based on reported forsterite and fayalite values (REUPDT) and were converted into oxide wt % of SiO_2, FeO, and MgO. The sum of the three oxides was fixed to that of the reported wt % sum of Fo and Fa, i.e., if Fo + Fa in a given experiment summed to 98 wt %, then the sum of SiO_2, FeO, and MgO for olivine from that experiment was also fixed at 98 wt %. Spinels compositions were estimated using the algorithm of Poustovetov and Roeder (2001). When Cr-spinel was included in the mass balance, the Cr content of the melt was set to zero. The model of Poustovetov and Roeder (2001) does not require a liquid Cr_2O_3 value and including Cr_2O_3 as an unknown in the melt leads to the Cr mass balance equation being under-constrained. The model does require FeO and Fe_2O_3 liquid values and thus Cr-spinel compositions were calculated simultaneously during the mass balance minimization. We also tested the liquid-magnetite model of Ariskin and Barmina (1999) for the more oxidized experiments, i.e., $\geq$QFM+1.75 (the model of Poustovetov and Roeder is not well calibrated under these more oxidizing conditions). When magnetite was used in the mass balance, liquid and bulk Cr_2O_3 contents were set to zero. For the six spinel-bearing experiments run at $\geq$QFM+1.75, the choice of which mass balance model to accept (Cr-spinel or magnetite) depended on which gave the lowest χ^2 value and a non-zero spinel mode. With two exceptions, the choice of Cr-spinel or magnetite had little effect on the calculated ol-liq K_D; in runs 7-1-654 and 6-1-654, ol-liq K_D decreased from 0.394 to 0.330 and 0.362 to 0.329, respectively when magnetite was used in place of Cr-spinel. For the four experiments that contained plagioclase, we used the model of Putirka (2005) to calculate a coexisting plagioclase composition. FeO and Fe_2O_3 contents in the liquid were calculated based on the following constraints: (1) FeO^{liq} +

0.89981 $\times Fe_2O_3^{liq} = FeO^{*liq}$ (as measured by microprobe); (2) $a_1 \times FeO^{liq} + a_2 \times FeO^{ol} + a_3 \times FeO^{sp} = FeO^{bulk}$; and (3) $a_1 \times Fe_2O_3^{liq} + a_3 \times Fe_2O_3^{sp} = Fe_2O_3^{bulk}$; where the a_1, a_2, and a_3 are the calculated mass fractions of the phases. Since sodium is known to be volatile in 1-atm experiments (e.g., Tsuchiyama et al., 1981), we allowed bulk Na_2O to vary in order to minimize χ^2; the closure constraint was applied to the bulk composition in that if bulk Na_2O decreased, the remaining oxides in the bulk increased by a proportional amount. Bulk ΔNa_2O values (the difference in percent between the bulk Na_2O content required to minimize χ^2 and the bulk Na_2O as measured by microprobe on the glassed starting material) for 22 of the mass balance calculations are less than the uncertainty on the sodium microprobe measurement (± 9%); for runs 10-4-654 and 7-2-C71, ΔNa_2O is 10.2% and 9.3%, respectively. It is clear from the liquid compositions that those experiments run in Al_2O_3 crucibles gained alumina. For these five experiments, we allowed the bulk Al_2O_3 to vary along with Na_2O and again the remaining oxide concentrations in the bulk increased or decreased depending on the relative changes in $Al_2O_3 + Na_2O$. For these five experiments, bulk ΔAl_2O_3 values range from ~5 to 31% and show a broad positive correlation with run temperature and run time. Uncertainties on the bulk, liquid, and solid phase compositions are based on the relative errors reported in Roeder and Emslie (1970). Specifically, fractional errors for SiO_2, TiO_2, Al_2O_3, FeO*, MgO, CaO, Na_2O and K_2O are 0.04, 0.04, 0.04, 0.04, 0.06, 0.05, 0.09, and 0.08, respectively (for olivine we lowered the uncertainty for MgO to 0.04 on the assumption that the high concentration of MgO in olivine would allow for more precise analyses). For Cr_2O_3 in Cr-spinel and the bulk composition we arbitrarily used a fractional error of 0.04. For the wet chemical FeO and Fe_2O_3 contents in the bulk composition, we used the FeO and Fe_2O_3 measurements and their reported uncertainties from Hill and Roeder (1974) to calculate fractional errors and plot them as a function of FeO and Fe_2O_3 concentrations—the data sets are well fit by the following equations: FeO fract. error = 0.050691/(FeO, wt %); R = 0.98 and Fe_2O_3 fract. error = 0.167676/(Fe_2O_3, wt %); R = 0.95. For the calculated Fe_2O_3 liquid contents, we used the expression above for the 1σ uncertainties since the uncertainties are rather large (for the range of bulk Fe_2O_3 measurements, fractional errors vary from 0.419 to 0.025). For the measured range of bulk FeO contents (5.3 to 10.8 wt %), fractional errors are substantial smaller than the FeO* microprobe uncertainty (0.01–0.005 vs. 0.04) and for this reason we added a constant term of 0.014 to the FeO fractional error equation when we applied it to the calculated FeO liquid contents. This brought the calculated errors on the liquid FeO concentrations more in line with the microprobe uncertainties but nevertheless allowed us to retain the concentration dependence.

Table A2. Compositions (in wt %) used for olivine-addition calculations

	SiO_2	TiO_2	Al_2O_3	Cr_2O_3	FeO*	MnO	MgO	CaO	Na_2O	K_2O	P_2O_5
MK low-Si[a]	48.75	2.63	13.89	0.044	11.57	0.169	7.89	11.30	2.42	0.393	0.215
MK high-Si[a]	51.40	2.44	13.46	0.045	10.43	0.166	7.39	11.24	2.22	0.383	0.202
ML[b]	51.90	2.04	13.84	0.051	10.41	0.166	7.62	10.70	2.22	0.339	0.206
Kil[c]	50.65	2.42	13.20	0.070	11.06	0.168	7.96	10.83	2.25	0.426	0.233

[a] Mauna Kea low-SiO_2 and high-SiO_2 compositions based on glass compositions with ≥7 wt % MgO reported in Stolper *et al*. (2004); Cr_2O_3 contents based on whole rock Cr vs. MgO regressions (Cr calculated at MgO values of 7.89 and 7.39 wt %, respectively); whole rock data from Rhodes and Vollinger (2004). Definition of glass and whole rock low-SiO_2 and high-SiO_2 compositions from Stolper *et al*. (2004).

[b] Mauna Loa composition represents the average of glass compositions with ≥ 7 wt % MgO from the GeoRock database (http://georoc.mpch-mainz.gwdg.de/georoc/). Cr content calculated from Mauna Loa bulk rock data (Rhodes, 1996) as described in the note for the Mauna Kea low-Si composition.

[c] Kilauea composition is the average of glass compositions from the GeoRock database with ≥ 7 wt % MgO.

Table A3. Compositions of calculated parental Hawaiian magmas (in wt %)

	K_D	$Mg\#^{ol}$	ΔQFM	SiO_2	TiO_2	Al_2O_3	FeO*	MnO	MgO	CaO	Na_2O	K_2O	P_2O_5
MK1	0.30	0.90	–0.5	47.09	2.11	11.18	11.73	0.17	15.52	9.15	1.94	0.32	0.17
MK1	0.30	0.90	–2.0	46.81	2.03	10.74	11.83	0.17	16.71	8.80	1.87	0.30	0.17
MK1	0.30	0.91	–0.5	46.77	2.00	10.60	11.60	0.17	17.30	8.68	1.84	0.30	0.16
MK1	0.30	0.91	–2.0	46.48	1.92	10.13	11.68	0.16	18.57	8.31	1.76	0.29	0.16
MK1	0.34	0.90	–0.5	46.53	1.94	10.29	11.92	0.16	17.93	8.44	1.79	0.29	0.16
MK1	0.34	0.90	–2.0	46.19	1.85	9.77	12.05	0.16	19.33	8.02	1.70	0.28	0.15
MK1	0.34	0.91	–0.5	46.17	1.82	9.65	11.75	0.16	19.92	7.92	1.68	0.27	0.15
MK1	0.34	0.91	–2.0	45.83	1.72	9.10	11.86	0.16	21.40	7.48	1.58	0.26	0.14
MK1	0.34	0.91	–1.0	46.04	1.78	9.43	11.79	0.16	20.50	7.75	1.64	0.27	0.15
MK2	0.34	0.91	–1.0	48.18	1.73	9.55	10.92	0.16	18.98	8.04	1.57	0.27	0.14
ML	0.34	0.917	–1.8	48.01	1.35	9.15	10.81	0.16	21.22	7.14	1.46	0.22	0.14
Kil	0.34	0.908	–0.7	47.74	1.74	9.49	11.37	0.16	19.02	7.84	1.61	0.31	0.17
Kil	0.34	0.908	–1.4	47.54	1.69	9.24	11.43	0.16	19.73	7.64	1.57	0.30	0.16

MK1 = Mauna Kea low-SiO_2 composition; MK2 = Mauna Loa high-SiO_2 composition; ML = Mauna Loa composition; Kil = Kilauea composition (all from Table A2). K_D is the constant value Fe^{+2}-Mg exchange coefficient between olivine and liquid used for each calculation; $Mg\#^{ol}$ is the Mg/(Mg+Fe), atomic, of the target olivine; ΔQFM is the fO_2 relative to QFM (O'Neill, 1987) used for each calculation. Starting with each average glass composition in Table A2, 0.0001 weight fraction of equilibrium olivine was repeated added to each composition until the evolving composition was in equilibrium with the target olivine; at each step Fe^{+3}/Fe^{+2} in the liquid was calculated using eqn. 12 of Jayasuriya *et al*. (2004), the specified fO_2, and the temperature calculated using the expression of Beattie (1993); olivine MnO and CaO contents calculated using the expression of Beattie *et al*. (1991) for MnO and a cation-based version of the algorithm of Libourel (1999) for CaO; cation-based Al and Cr partition coefficients between olivine and liquid were 0.005 and 0.6, respectively (Bédard, 1994). Parental Cr_2O_3 contents not listed. See the main text for a discussion of the target olivine compositions and fO_2s of Hawaiian lavas.